

University of Windsor

Scholarship at UWindor

Electronic Theses and Dissertations

Theses, Dissertations, and Major Papers

1-1-1969

Direct field electrotransport of carbon in gamma iron.

Emilio Alfred Falquero
University of Windsor

Follow this and additional works at: <https://scholar.uwindsor.ca/etd>

Recommended Citation

Falquero, Emilio Alfred, "Direct field electrotransport of carbon in gamma iron." (1969). *Electronic Theses and Dissertations*. 6067.

<https://scholar.uwindsor.ca/etd/6067>

This online database contains the full-text of PhD dissertations and Masters' theses of University of Windsor students from 1954 forward. These documents are made available for personal study and research purposes only, in accordance with the Canadian Copyright Act and the Creative Commons license—CC BY-NC-ND (Attribution, Non-Commercial, No Derivative Works). Under this license, works must always be attributed to the copyright holder (original author), cannot be used for any commercial purposes, and may not be altered. Any other use would require the permission of the copyright holder. Students may inquire about withdrawing their dissertation and/or thesis from this database. For additional inquiries, please contact the repository administrator via email (scholarship@uwindsor.ca) or by telephone at 519-253-3000ext. 3208.

UNIVERSITY OF WINDSOR
DEPARTMENT OF ENGINEERING MATERIALS

Direct Field Electrotransport of Carbon in Gamma Iron

A Thesis

Submitted to the Faculty of Graduate Studies
in Partial Fulfillment of the Requirements
for the Degree of Doctor of Philosophy

by

EMILIO ALFRED FALQUERO

WINDSOR, ONTARIO, CANADA

NOVEMBER, 1969

UMI Number:DC52634

UMI[®]

UMI Microform DC52634
Copyright 2007 by ProQuest Information and Learning Company.
All rights reserved. This microform edition is protected against
unauthorized copying under Title 17, United States Code.

ProQuest Information and Learning Company
789 East Eisenhower Parkway
P.O. Box 1346
Ann Arbor, MI 48106-1346

ABX 6588

UNIVERSITY OF WINDSOR
FACULTY OF GRADUATE STUDIES

The undersigned certify that they have read, and recommend
to the Faculty of Graduate Studies for acceptance, a thesis
titled

DIRECT FIELD ELECTROTRANSPORT OF CARBON IN GAMMA IRON
submitted by EMILIO ALBERTO FALQUERO
in partial fulfillment of the requirements for the degree of
Doctor of Philosophy.

W. J. ...
.....
Supervisor

J. K. ...
.....

[Signature]
.....

Clara ...
.....

A. G. Smith
.....

H. B. Huntington
.....
External Examiner

November 21, 1969
.....
Date

ACKNOWLEDGEMENTS

Dr. W. V. Youdelis has been an unfailing source of guidance and advice; it has been a pleasure and a privilege to have been associated with him in the present investigation. The author is also indebted to the many individuals in the Department of Engineering Materials who have contributed advice and loaned equipment. In particular, thanks are extended to Dr. G. Cochrane for his comments and criticisms, and to Professor R. G. Billinghurst for his considerate departmental supervision.

The financial assistance of the National Research Council in the form of a Research Grant (#670) is also gratefully acknowledged.

CONTENTS

	Page
ABSTRACT.....	vi
INTRODUCTION.....	1
ELECTROTRANSPORT.....	5
A. THEORIES.....	5
B. DIRECT FIELD EXPERIMENTAL TECHNIQUES.....	9
C. RESULTS.....	13
EXPERIMENTAL PROCEDURE.....	19
A. MICROHARDNESS CALIBRATION.....	19
1. Preparation of Standards.....	19
2. Microhardness measurements.....	21
3. Carbon Analysis.....	21
B. ELECTROTRANSPORT SPECIMEN PREPARATION.....	23
1. Carburisation.....	23
2. Welding.....	23
C. APPARATUS.....	26
1. Vacuum Furnace.....	26
2. Measuring Circuit.....	28
D. ELECTROTRANSPORT RUN PROCEDURE.....	34
E. ANALYSIS.....	36
RESULTS.....	39
DISCUSSION OF ERRORS.....	61
A. ERRORS IN TEMPERATURE AND DIFFUSIVITY.....	61
1. Temperature Measurements.....	61
2. Diffusivity.....	67

Table of Contents (cont'd)

	Page
APPENDIX V. Sample Calculation.....	107
VITA AUCTORIS.....	109

ABSTRACT

In direct field electrotransport at low field strength the effective charge of carbon in gamma iron varies with the applied field. At 950°C the charge is 4.5 ± 0.5 at a field of 0.106 V cm^{-1} , rising to a value of 13.6 ± 1.4 at 0.028 V cm^{-1} , and falling rapidly at lower fields. Similar results are encountered at 920 and 980°C; the temperature dependence of the total effective charge is not marked. It is proposed that carbon transport occurs by two processes: vacancy transport, which is activated by a field of 0.028 V cm^{-1} but is field independent at higher fields, and interstitial transport, the velocity of which is proportional to the applied field. At low fields (near 0.028 V cm^{-1}) the vacancy mechanism determines the transport rate; at higher fields interstitial transport becomes significant, and may be dominant at fields larger than 1.0 V cm^{-1} . The rate of vacancy transport is determined by an activation energy of 42 kcal mol^{-1} . The effective charge for purely interstitial carbon electrotransport is strongly temperature dependent; charge values of 2.5, 1.5 and 0.6 were obtained at 920, 950 and 980°C respectively.

INTRODUCTION

When an electric field is applied across a metal or an alloy the salient effect is the flow of electrons. However, the ion cores in the metal, being positively charged, will also move under the influence of the electric field. This effect is known as electrotransport.

The determination of ionic charge values is of considerable importance since they provide some insight into the electronic band structure and the nature of the crystalline bond in metals and alloys. It is recognised that the strength of the interatomic bond is a significant factor in determining the high temperature properties of alloys. Thus electrotransport techniques are applicable in the development of alloy theory and the investigation of new kinds of steels and heat resistant alloys.

Electrotransport is also of practical interest in the field of microcircuit engineering, where failures in thin film and wire conductors due to electrotransport have been reported. Such large macroscopic effects are rare in solids since the mobility of the ions is relatively small and it is only after prolonged electrotransport that substantial redistribution of material can occur. However, in liquid metals and alloys the ionic mobilities are much larger and the separation of isotopes or alloying components by the process of electrotransport is feasible.

The motion of the ions is not determined solely by the

magnitude of the ion charge and the applied electric field; collisions between charge carriers and ions occur, with a resulting transfer of momentum to the ions. The electron-ion and hole-ion momentum transfer effects are appreciable and frequently determine the rate and direction of ion transport. In electrotransport calculations the ions are usually considered to have an "effective charge", which is not the true charge of the ions but rather a net term comprising the true charge and the momentum transfer contribution from electrons and holes. The "true charge" is that positive charge on the ions arising from the loss of outer electrons to the Fermi pool.

Separate measurements of true and effective charges would be quite desirable, but true charges are difficult to measure directly. Bibby and Youdelis¹ were able to measure the charges of carbon and nitrogen in iron, obtaining values of +4.3 and +5.7 respectively, which are in satisfactory agreement with the valencies or group numbers of these elements in the periodic table. The experiments comprised solute transport across an equilibrated two-phase region under a Hall field. Thus the motion of the ions in the direction of the Hall field was unaffected by momentum transfer effects due to the direct current. Presumably the charges so obtained were the true charges, or as close to the true charges as yet measured. Unfortunately, the number of systems which may be studied in this manner is severely limited since the method requires an alloy of high Hall coefficient which also exhibits a two-phase region at suitable concentration and temperature levels. In the present experiment

an attempt at extending the method of Hall field electrotransport to iron-based ternary alloys was made and the difficulties already noted were encountered. Moreover, accurate phase equilibrium data is essential in this technique, and since ternary alloy equilibrium diagrams are seldom known with great accuracy separate experiments would have been required to determine at least a portion of these diagrams for the systems to be studied.

Smolin and Frantsevich² have proposed a different approach for determining true charge. They develop equations expressing the effective charge of solute or solvent ions as functions of the alloy concentration and temperature. Thus the true charge may be calculated from effective charge values determined over a range of temperature and concentration. Experiments by Smolin et al³⁻⁸, appear to support the validity of this approach for several metals and alloys. Bibby et al⁹ found that the effective charge of carbon in gamma iron increased from +8.6 at 950°C to +13.7 at 842°C, which is in qualitative agreement with the theory of Smolin and Frantsevich.

Despite such promising developments, it appears that the present knowledge of electronic scattering mechanisms in metals will require further advances before true charges may be reliably determined from effective charge data. Moreover, the many practical problems encountered in microcircuits, as a result of electrotransport of material or void migration, indicate the need for more extensive and intensive investigations of the electrotransport mechanisms. This investigation is primarily concerned with the determination of the effective

charge of carbon in gamma iron under different experimental conditions, and the possible relation of this data to the true charge. The relative stability of the iron-carbon system and the fairly high mobility of interstitial carbon make this system eminently suitable for electrotransport study. Results in the literature indicate a rather large scatter in the cited values of effective charge of carbon in iron⁹⁻¹². This suggested the desirability of testing whether the magnitude of the effective charge of carbon was influenced by experimental parameters not normally considered in the theoretical equations of electrotransport. In particular, the effect of current density variation was studied. Electrotransport in nitrogen-iron alloys was also investigated but due to experimental difficulties associated with the high temperature instability of this system no conclusive results were obtained.

ELECTROTRANSPORT

A. THEORIES

A large number of theories have been proposed in an attempt to explain quantitatively the phenomenon of electrotransport. In calculating the force on the ion due to an applied electric field the main problem arises when the electron interaction force is introduced. Generally a quantitative description of electrotransport is approached phenomenologically, using irreversible thermodynamics, or on an atomic level, by calculating the momentum transfer between electrons and ions.

The equation of Ficks¹³ has achieved considerable popularity, particularly among Russian investigators who tend to adopt the reasoning leading to Ficks' basic equation and make only minor modifications or improvements on this. Ficks' theory is based on an atomistic model whereby the contribution of momentum transfer to the ion due to electron-ion collisions is calculated directly from scattering parameters. Mass transport is assumed to be determined by the motion of thermally activated ions. Ficks' treatment neglected to take into account the effect of positive charge carriers or holes on the effective charge of the ion, and this was remedied by Glinchuck¹⁴ who introduced a hole-ion interaction term. Thus the Ficks-Glinchuck equation for the total force on the ion is given by:

$$F_i = eE (q_i - n_- l_- \sigma_- + n_+ l_+ \sigma_+) \quad (1)$$

where n , l and σ are density, mean free path and scattering

cross section for the electrons (-) and holes (+). Other terms are the applied electric field (E), the electronic charge (e) and the true charge of the ions (q_i). The bracketed terms comprise the parameter defined as the "effective charge".

In an excellent review article by Verhoeven¹⁵ the more prominent theories of electrotransport are summarised and compared. It is interesting to note that theories based on quite different premises often arrive at very similar expressions for the force on the ion. Klemm¹⁶ has approached the problem from irreversible thermodynamics, writing Onsager equations for the forces on the ions (in interstitial and self transport) as functions of the fluxes. This treatment is somewhat similar to the phenomenological derivation of Mangelsdorf¹⁷ who assumes the force on the ions in dilute molten alloys is proportional to the electron flux, the proportionality constant being arbitrarily defined as a friction coefficient. The similarity in the general equations obtained by Klemm and Mangelsdorf is not unexpected, but it is noteworthy that in the case of transport by activated ions both these equations are analogous to that obtained by Ficks, whose derivation was based on an atomistic rather than a phenomenological approach.

In the theory of Huntington and Grone¹⁸ a quantum mechanical approach is used. The force on the ion during self transport is calculated from the rate of momentum transfer between electrons and defects, assuming that electrons are scattered by defects only. This force, which is expressed as a function of the relative resistivities of defect and lattice sites and the ratio

of the electron mass to the magnitude of the electron effective mass, was considered to be always anode directed, whether the predominant charge carriers were electrons or holes. In a later publication Huntington and Ho¹⁹ made a small but significant correction to the theory, showing that the direction of the friction force depended on the sign of the electron effective mass. Where the defects are taken to be interstitial ions Huntington's expression for the force on the ion is comparable to that of Ficks. A quantum mechanical derivation centered on defect scattering has also been used by Bosvieux and Friedel²⁰, but the results are only claimed to be approximated quantitative.

The theories of Ficks, Klemm, Mangelsdorf and Huntington all show that the electrotransport of an ion is determined both by its charge and the electron and hole momentum transfer. On the other hand Bosvieux's theory for interstitial transport and Mangelsdorf's result for infinitely dilute solutions are contrary to other theories and suggest that the rate of electrotransport of an interstitial ion is unaffected by its charge.

The appeal of Equation (1) lies in its explicit definition of the electron and hole contributions to the electrotransport process. The major disadvantage is that the expression for the force on the ion is somewhat complicated, and theoretical calculations become correspondingly more difficult. Equations other than the Ficks-Glinchuck equation usually contain only one interaction term, a sort of net effect term which may be positive or negative according to the sign of the effective mass of the charge carriers.

Recently Smolin and Frantsevich² have elaborated on the Ficks-Glinchuck equation. Interpreting the mean free paths in terms of resistivities, and assuming that the overall resistivity varies linearly with temperature ($\rho = \rho_0 + \alpha T$)*, they express the effective charge as a hyperbolic function of the factor $(T + \rho_0 / \alpha)^{-1}$. A corresponding equation relating the effective charge of a component in an alloy to its concentration is also derived. In the special case where the ratio of the overall carrier conductivity (electrons and holes) to the electron conductivity is independent of temperature, the effective charge becomes a linear function of the factor $(T + \rho_0 / \alpha)^{-1}$. Experimental results by Smolin et al⁴⁻⁸ appear to support the conclusions of Smolin and Frantsevich for electrotransport in pure silver, nickel and iron, and also in molybdenum-tungsten and nickel-molybdenum alloys. However, it must be noted that the general equation for the effective charge is quite complex, containing partial resistivities and scattering cross sections for electrons and holes. It would be dangerous to assume that the relation of effective charge to the factor $(T + \rho_0 / \alpha)^{-1}$ will always be either hyperbolic or linear for any metal or alloy. Perhaps the greatest weakness of this theory is that for the evaluation of true charge it is necessary to perform an extrapolation to the limit $(T + \rho_0 / \alpha)^{-1} = 0$. Effective charge measurements are usually made over a relatively narrow range (typically 900°C to 1300°C) so that the extrapolation covers an interval several times larger than the range over which the

* Smolin's ' α ' is not to be confused with the usual temperature coefficient of resistivity defined by $\rho = \rho_0(1 + \alpha T)$.

results are taken, thus causing rather large errors in the calculated values of true charge.

The force on the ion, and thus the effective charge, is not directly obtainable experimentally, but rather has to be calculated from available experimental data such as ion velocity or mobility. This is usually accomplished through the Einstein relation for absolute mobility (U_i) in terms of the diffusion coefficient (D_i), viz.

$$U_i = D_i/kT \quad (2)$$

where k is Boltzman's constant and T is the absolute temperature. The denominator of this expression is sometimes modified by a correlation coefficient to account for the lack of diffusion jump randomness due to the crystalline nature of the lattice. Defining the absolute ionic mobility as velocity per unit force, the ion velocity may be given in terms of the Ficks-Glinchuck equation:

$$v_i = \frac{D_i e E}{kT} (q_i - n_{-} l_{-} \sigma_{-} + n_{+} l_{+} \sigma_{+}) \quad (3)$$

Thus the effective charge of the ion may be calculated directly from its drift velocity under an applied field.

B. DIRECT FIELD EXPERIMENTAL TECHNIQUES

Perhaps the simplest type of electrotransport experiment is that in which an initially homogeneous wire is subjected to an electric field. The resulting transport may be measured by metallographic observation, wet chemical analysis, weighing

techniques or the movement of inert markers. In the case of alloys a section of known composition can be butt welded between sections of different composition (or pure material) to form a sandwich-type diffusion couple, and the component under study allowed to diffuse in both directions, with and against the applied electric field. The difference in penetration at the two welds will give a measure of the electrotransport velocity. This method has the advantage that all the migration occurs over a small region of fairly uniform temperature.

The method using superimposed chemical diffusion and electrotransport is used in the present investigation. A brief description of the mathematical formulation is given. Where both chemical diffusion and electrotransport occur the motion of the ions is described by a linear partial differential equation (Boltaks²¹);

$$\frac{\partial C}{\partial t} = D \cdot \frac{\partial^2 C}{\partial x^2} - v \cdot \frac{\partial C}{\partial x} \quad (4)$$

where C , t and x are concentration, time and distance. The electrotransport velocity (v) and the diffusion coefficient (D) are assumed to be independent of concentration. Consider the case represented in Figure 1, where the concentration of the component under investigation in the central region (between the welds) is initially C_0 and zero elsewhere. Assuming that the effective charge is positive and the semi infinite boundary conditions are applicable, the penetration concentration profile at the cathode is given by a solution of Equation (4);

$$C = \frac{C_0}{2} \left(1 - \operatorname{erf} \left(\frac{x - vt}{2 \sqrt{Dt}} \right) \right) \quad (5)$$

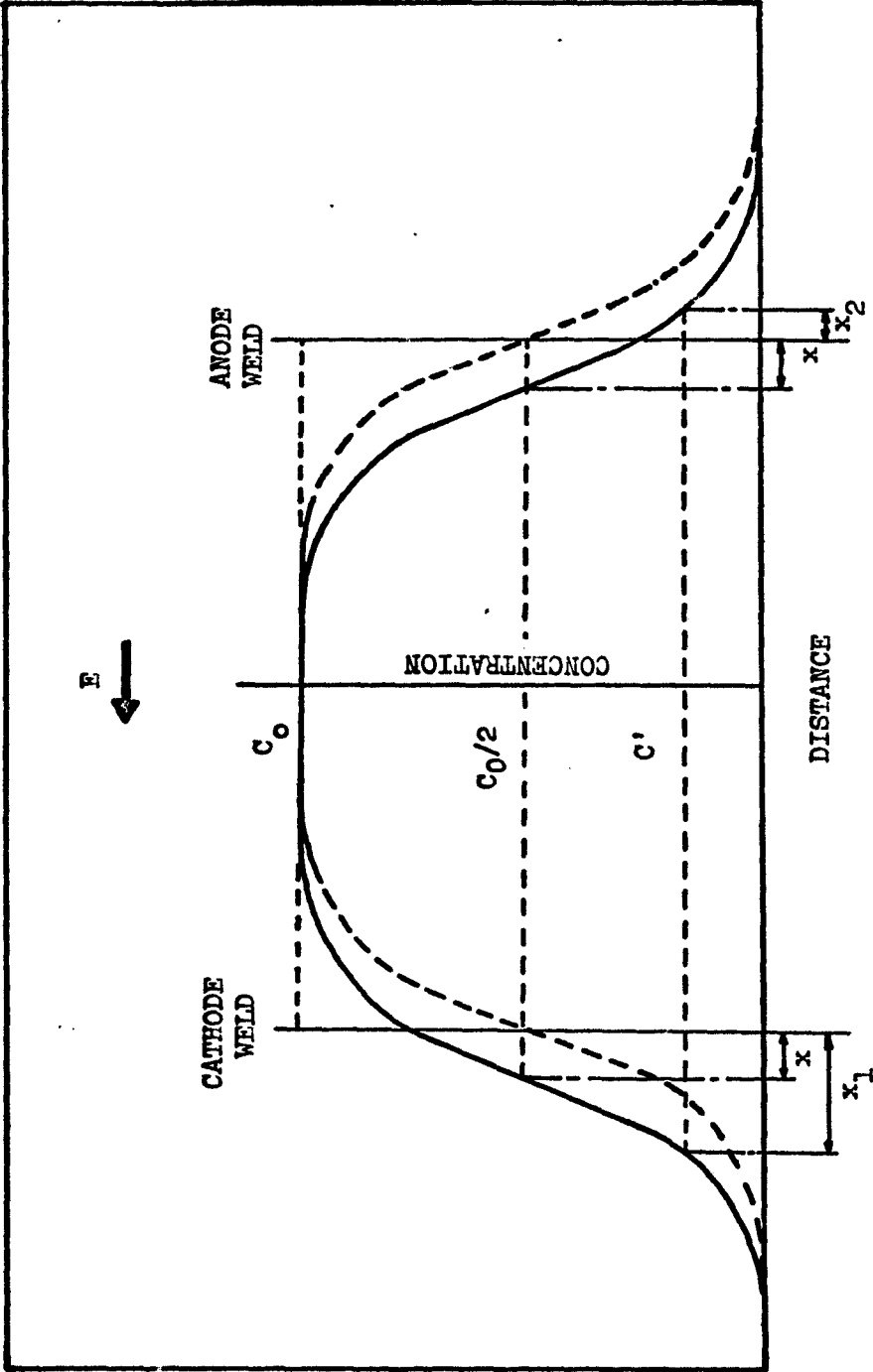


Figure 1. Penetration profiles under combined chemical diffusion and electrotransport (full line), and under chemical diffusion only (broken line).

where v is the electrotransport velocity. The motion of a plane of constant composition may be obtained by imposing the condition

$$dC = \left. \frac{\partial C}{\partial x} \right|_t \cdot dx + \left. \frac{\partial C}{\partial t} \right|_x \cdot dt = 0 \quad (6)$$

The partial differential terms may be calculated from Equation (5) and the resulting differential equations solved to give:

$$x = K \sqrt{Dt} - vt, \quad K = \text{constant} \quad (7)$$

A similar calculation for migration at the anode gives:

$$x = K \sqrt{Dt} + vt. \quad (8)$$

Physically, this implies that the chemical potential and field forces operate independently.

If the distances of planes of specific compositions (C') from the cathode and anode welds respectively are x_1 and x_2 , then the velocity of electrotransport is given directly as:

$$v = \frac{x_1 - x_2}{2t} \quad (9)$$

Alternately v may be obtained by measuring (at either weld) the distance between the plane of concentration $C_0/2$ and the weld.

The penetration curves may be measured by electron microprobe analysis. However, analysing for carbon in iron requires operating a probe at the limit of operational accuracy, and in this case more reliable results may be obtained by microhardness analysis. In iron-carbon martensite the hardness is a linear function of composition over the approximate range 0.08 to 0.45 weight per cent carbon^{9,12}.

Recently Russian investigators have developed a technique using radioactive tracers which appears to be quite accurate. Irradiated isotopes are introduced into the central region of a wire and the subsequent electrotransport is monitored by radiation counters. The advantage of this technique is that it may readily be used with interstitial or substitutional alloys or in pure metals.

C. RESULTS

In 1861, Gerardin²³ first reported an electrotransport effect in molten binary alloys. Electrotransport in solids was not investigated until the 1930's, when Seith et al^{24,25} reported on the migration of carbon and nitrogen in iron, and Johnson²⁶,²⁷ reported evidence of self transport in a number of metals. Following the development of the various electrotransport theories and the improvement of experimental techniques, experimental results began to acquire a certain consistency. Experimental determinations of the effective charge in self transport by several investigators, summarised in Table I, are in reasonable agreement. The apparent variation of effective charge with temperature appears to be well documented. Kuz'menko et al^{28,29,30} and Smolin et al^{5,6,7} calculated true charges from effective charge data at different temperatures. Their results agree closely, particularly the value of +0.86 which both obtained for the true charge of silver.

It is generally assumed that metals which have been shown to be p-conducting in Hall field experiments should exhibit

TABLE I

Effective Charge values for Self-transport

Metal	Temperature °C	MEASURED EFFECTIVE CHARGES			
		Wever 31,32	Grone 33	Kuz'menko et al ³⁰	Smolin et al ⁵⁻⁷
Cu	800	-	-5.0	-	-
	900	-14.0	-2.0	-38.0	-
	1000	+12.0	0	-22.0	-
Ag	750	-	-	-26.0	-20.0
	800	-	-	-27.0	-19.0
	875	-	-	-22.0	-
	900	-	-	-	-17.0
Ni	1000	-	-	-	- 4.5
	1200	- 5.8	-	-	- 3.8
	1300	- 1.8	-	-	- 3.3
	1385	- 1.5	-	-	- 3.1
Fe	1000	-	-	-	+ 7.2
	1190	+43.0	-	-	-
	1300	+12.0	-	-	-
	1325	+ 9.0	-	-	-
	1350	-	-	-	+ 3.7

cathode directed electrotransport. This is contradicted by the work of Kuz'menko who found self transport in zinc, cadmium and tin to be anode directed.

Electrotransport in copper is particularly interesting as there is a reversal in the sign of the effective charge as the temperature is increased. The results of Wever^{31,32} and Grone³³ indicate a negative charge for copper at lower temperatures which becomes positive when the temperature is increased above about 1000°C. To account for this it might be postulated that the ratio of scattering cross sections for holes and electrons varies with temperature, and that the direction of electrotransport is determined by the magnitude of the ratio $n_{+1}\sigma_{+}/n_{-1}\sigma_{-}$. Such a mechanism might also explain the negative effective charges of p-conducting metals.

Both Huntington¹⁸ and Kuz'menko have found that the velocity of self transport and the current density are linearly related, indicating that the effective charge is not a function of the applied field. However, Seith and Wever³⁴ found the mobility to be a non-linear function of current density in copper-aluminum and silver-zinc alloys.

Electrotransport in substitutional alloys poses new problems since both components participate in the process. The molybdenum-tungsten system, which exhibits complete solid solubility was studied by Smolin⁴ over wide ranges of temperature and composition. The effective charge of molybdenum was negative, whereas that of tungsten was positive. From the temperature variation of the effective charge true charges were calculated.

It was found that at all compositions the true charge of the minor component was negative and that of the major component was positive; at 50 atomic per cent both components had zero true charge.

In alloys where several phases occur the effective charge may be different for each phase. Seith and Wever³⁴ found that the direction of migration in aluminum-copper alloys changed from anode to cathode going from the beta to the gamma phase, as a consequence of a change from n- to p-conduction.

The study of electrotransport in interstitial alloys offers some experimental advantages. Due to the relatively high mobility of most interstitial elements experiments may be of shorter duration than in self transport, and the true mobility may be obtained directly if it can be assumed that the much less mobile atoms of the matrix act as a fixed frame of reference. The presence of interstitials will also have a pronounced effect on the relative charge of the matrix ions. It was noted in Table I that pure iron has a positive effective charge, yet Frantsevich et al^{35,36} and Gertstriken et al³⁷ found that in iron carbon alloys the effective charge of iron is negative.

The results of several observations of the transport of carbon in iron are summarised in Table II. Darken and Dayal¹⁰ were unable to obtain a consistent temperature variation of effective charge, probably due to experimental errors. The results of Kalinovich¹² and Bibby et al⁹ indicate a variation of effective charge with temperature as in self transport experiments, although the charges reported by Kalinovich are almost a

TABLE II

Values of Effective Charge for Carbon in Iron

Temperature °C	Effective Charge q_{eff}	Reference
1124 1175 1226	+ 4.9 + 2.6, + 3.5 + 2.7, + 3.9	Darken & Dayal ¹⁰
950 1000 1050 1100 1150	+ 13.4 + 11.0 + 7.0 + 10.6 + 8.1	*Kalinovich ¹²
842 902 925 950	+ 13.7 + 9.3 + 8.9 + 8.6	Bibby et al ⁹
950 1000 1050 1100 1150	+ 1.7 + 1.6 + 1.0 + 1.4 + 1.1	* Frantsevich et al ³⁶

* Note: The values given by Kalinovich¹² may have been calculated from the original results of Frantsevich et al³⁶.

factor of two larger than those obtained by Bibby. Frantsevich and Kovenskii³⁸ claim to have obtained accurate data for the transport of carbon in iron, nickel and cobalt. The actual values of effective charge were not reported, but it was stated that in all cases the effective charge of carbon was related hyperbolically to the factor $(T + \rho_0/\alpha)^{-1}$, and a true charge of +3.7 was calculated for carbon in gamma iron. This is comparable to the value of +4.3 obtained by Bibby and Youdelis¹ for the true charge of carbon in alpha iron in Hall field electrotransport experiments.

The effective charge of nitrogen in gamma iron has been found to be negative. Seith and Daur²⁵ encountered severe experimental difficulties due to the inherent high temperature instability of the iron-nitrogen system, and were only able to report qualitatively that nitrogen migrated towards the anode. Bibby et al^{1,9} reported an effective charge of -14.0 (at 922°C) in direct field electrotransport and a true charge of +5.7 (at 736°C) in Hall field electrotransport for nitrogen in gamma and alpha iron respectively.

EXPERIMENTAL PROCEDURE

Specimens consisting of carburised iron wire, butt welded between sections of pure iron wires, were diffusion annealed in a vacuum furnace. A direct current through the specimen provided an electric field for electrotransport. Variable specimen temperatures were obtained through a combination of Joule heating (due to the specimen current) and external furnace heating. Chemical diffusion and electrotransport occurred simultaneously, the difference in diffusion penetration at the anode and cathode welds providing a measure of electrotransport velocity. Carbon concentrations were measured by a microhardness technique, using a calibration curve of hardness versus carbon content in martensite.

A. MICROHARDNESS CALIBRATION

1. Preparation of Standards

Sections of Armco iron strip (see Appendix I for analysis) measuring 0.1" x 0.5" x 1.5" were carburised at 925°C in a Multiple Unit vertical resistance furnace. A Honeywell Servotronic (Model 5500101-2-04) temperature controller and a chromel-alumel thermocouple were used to control the furnace temperature. The controller was room temperature compensated and operated a relay to select high or low power. With this unit the specimen temperature could be reproduced within 2°C and maintained accurately with a cycle of $\pm 1^\circ\text{C}$ about the mean temperature. The specimen was suspended by a Nikrothal wire inside a 1.25"

diameter quartz tube which also contained the controlling thermocouple and was provided with facilities for atmosphere control.

In the carburising operation the specimen was first introduced into the cold zone of the tube and the system flushed with argon for one minute, then flushed with methane (technical grade) for another minute. The specimen was then raised to the central hot zone of the furnace and the methane flow rate reduced to 10-12 cc/min. A total of twelve standards were prepared with carburisation times ranging from 20 to 210 minutes. Carburisation was terminated by lowering the specimen into the cold zone of the chamber and allowing it to cool slowly.

The edges of the sample were then ground down so that in the subsequent homogenisation treatment only carbon which had penetrated through the large flat surfaces of the sample was available for redistribution. The amount of material removed from the edges varied from 0.02" to 0.1" according to the estimated depth of carbon penetration.

A five hour anneal at 1000°C was sufficient to render the sample completely homogeneous. During this treatment the samples were protected from oxidation and decarburisation by a double envelope of Sen-Pak heat treating foil and an argon atmosphere. A horizontal furnace with a 1.5" diameter quartz tube chamber and a Honeywell (Model R7086-1488-2) temperature controller was used in this operation. The temperature was controlled to within 5°C.

Each specimen was then sectioned transversely into three approximately equal parts. The outer sections were retained for

chemical analysis. The central sections were austenised 10 minutes at 925°C under argon in the vertical Multiple Unit furnace and then quenched into iced brine. Some surface decarburisation occurred during this treatment and the affected region (about 0.005" depth) was removed by grinding. The samples were then mounted in bakelite and polished in preparation for metallographic and microhardness analyses. The samples all exhibited a regular martensitic structure (see Figure 2) after etching in 2% nital solution.

2. Microhardness Measurements

Hardness measurements were made in a Leitz Durimet Microhardness Tester using a 500 gm load. For each specimen about twenty indentations were made, these being arranged in a loose grid designed to sample all the exposed surface. Mean hardness values and standard deviations were calculated for each specimen. The relatively small deviations obtained, supported by metallographic observation, indicated good carbon homogeneity.

In a trial sample hardnesses were measured both on a flat surface and on the cross-section, giving values of 523 ± 50 VPH and 552 ± 50 VPH respectively. This showed that no significant errors were introduced by making measurements on a side rather than a cross-section.

3. Carbon Analysis

The outer sections of the homogenised samples were machined into flakes and analysed for carbon content in a Leco Carbon Analyser (Model 507-100). Extreme care was taken to avoid

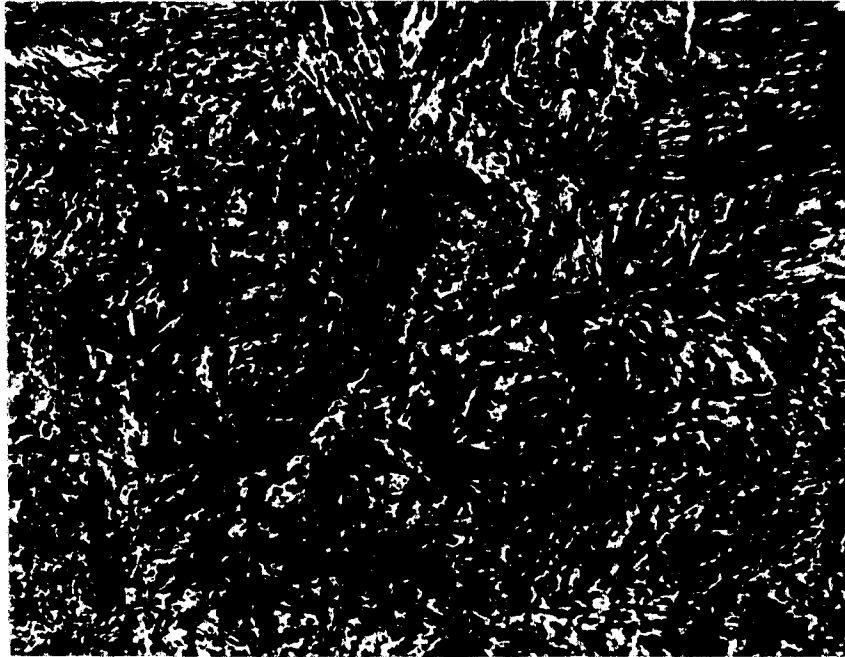


Figure 2. Typical martensitic structure
obtained after carburisation and
homogenisation. x 600

contamination in the machining process and other handling operations.

The analysis was carried out in split sequence, alternating samples to be tested with standard samples (obtained from the U.S. National Bureau of Standards) of reasonably close composition. The correspondence between measured carbon concentrations for the USNB Standards and the actual concentrations (shown in Table III) indicates that analysis errors were negligible.

B. ELECTROTRANSPORT SPECIMEN PREPARATION

1. Carburisation

Iron-carbon wires for electrotransport experiments were prepared by carburisation and homogenisation following the procedure adopted for the preparation of standards for micro-hardness calibration. Sections of 0.045" diameter Armco iron wire, about 1.5" long, were carburised for 20 minutes at 925°C under methane, and then homogenised for 3 hours at 1000°C. The resulting wire exhibited a uniform carbon concentration of about 0.5 wt.% (2.3 at.%).

2. Welding

Sections of carburised wire measuring about 0.25" in length were butt welded between two 3" sections of pure iron wire of the same diameter using a Rocky Mountain Spot Welder Model 506 (shown in Figure 3). The faces to be welded were prepared by grinding successively on grades 240, 320 and 600 Diamond Grit paper, care being taken to insure that the ground surface was perfectly flat and perpendicular to the axis of the wire. The

TABLE III

Standard Code	Measured Concentration of Carbon, wt.%	U. S. Nat. Bur. Standards, Carbon Concentration, wt.%
8i	0.074 0.079 0.075	0.077
11g	0.191 0.190 0.189	0.191
32e	0.402 0.406 0.399	0.409
13f	0.632 0.615 0.622	0.629
14d	0.832 0.836 0.834	0.841

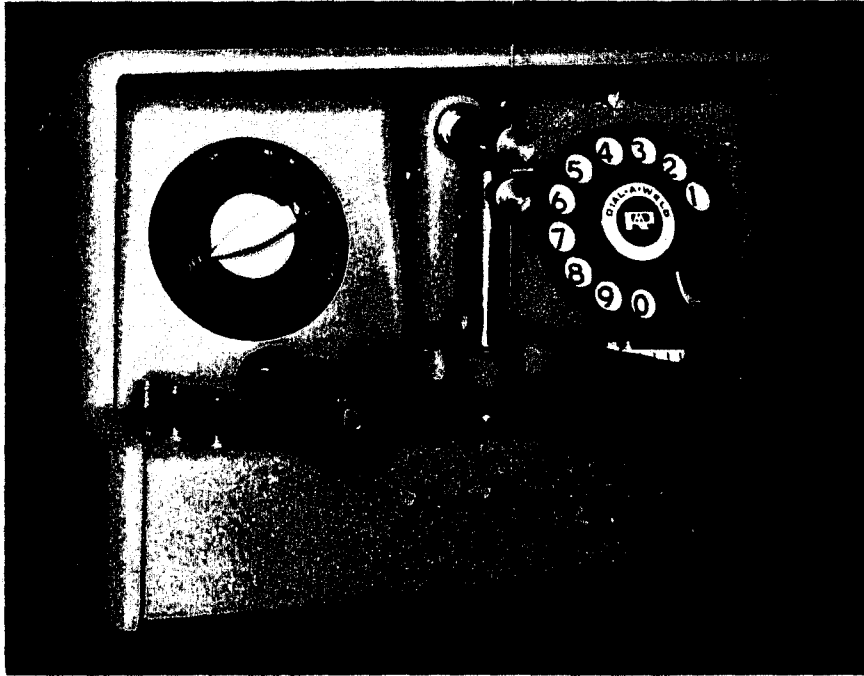


Figure 3. Spot welder, with specimen in position for butt welding.

regular electrodes of the welder were replaced by the wires and a weld formed by discharging a pulsed current through the wires. Adjustments for current, discharge time and load pressure permitted a large variation in the type of weld obtained. Welds were cleaned in dilute hydrochloric acid and examined in a low power binocular microscope. Any samples with imperfect or misaligned welds were rejected. Figures 4(a) and (b) illustrate typical welds. The small amount of oxide particles present (only apparent after over-etching and repolishing) were considered desirable since they served as inert markers defining the weld interface.

C. APPARATUS

1. Vacuum Furnace

A furnace was built into the vacuum chamber of a JEOLCO Evaporator (Type JEE-4B). The furnace consisted of a Kanthal heating element wound around a 0.75" diameter quartz tube, perforated stainless steel end plates and four concentric stainless steel, thin walled tubes which acted as heat reflectors. The outer reflector was 4" in diameter and was surrounded by a water cooled coil of 0.25" diameter copper tubing. The length of the furnace was four inches.

The nickel plated base plate of the vacuum chamber was provided with water cooled feed-throughs for power and thermocouple connections. A large glass bell jar enclosed the system, sealing against the base plate with an 'O' ring. The bell jar was protected from radiated heat by tantalum foil baffles and a



Figure 4(a), Weld interface before diffusion, x 100

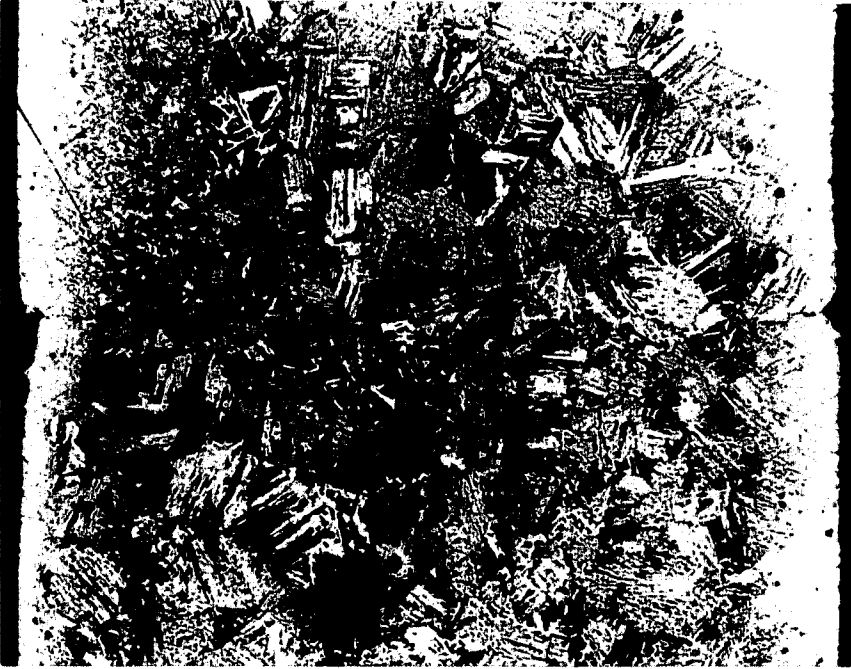


Figure 4(b), Weld interface after diffusion, x 100

foil lining; it was also cooled externally by a stream of air and a water cooled copper coil placed next to the 'O' ring seal. Three views of the furnace are shown in Figures 5(a), (b) and (c). Under operating conditions a vacuum of 3×10^{-5} to 7×10^{-5} Torr could be obtained in the furnace.

A furnace temperature of about 1000°C was reached with a heater element current of 23 amperes (a.c.), and this temperature could be maintained indefinitely without overheating the power leads, seals or bell jar. A specimen temperature of 1000°C could be reached using various combinations of specimen current and heater current, as shown in Figure 6. Power to the furnace was supplied by a variable autotransformer; the specimen current was provided by a Hewlett Packard D.C. Regulated Power Supply (Model 6260A) with a constant voltage load regulation of 0.01% and a ripple of less than 1 mVrms.

2. Measuring Circuit

The specimen temperature in the carburised region was measured by three (0.003" diameter) wire probes spot welded to the specimen as shown in Figure 7, since the voltage gradient along the sample would render inaccurate temperature measurements made with a simple thermocouple. The two outer chromel probes were connected through fixed resistances and a variable tap resistance as shown in Figure 8. This balancing circuit was adjusted until the output voltage remained unchanged when the direction of the specimen current was reversed. At this stage the circuit was properly balanced and the true temperature was indicated. The outer chromel probes were also tapped and the

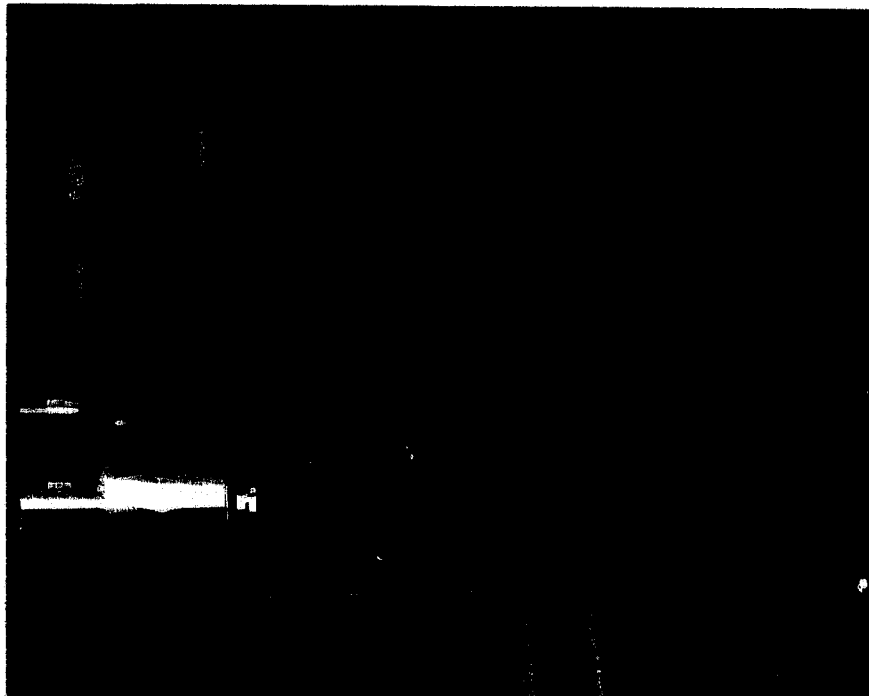
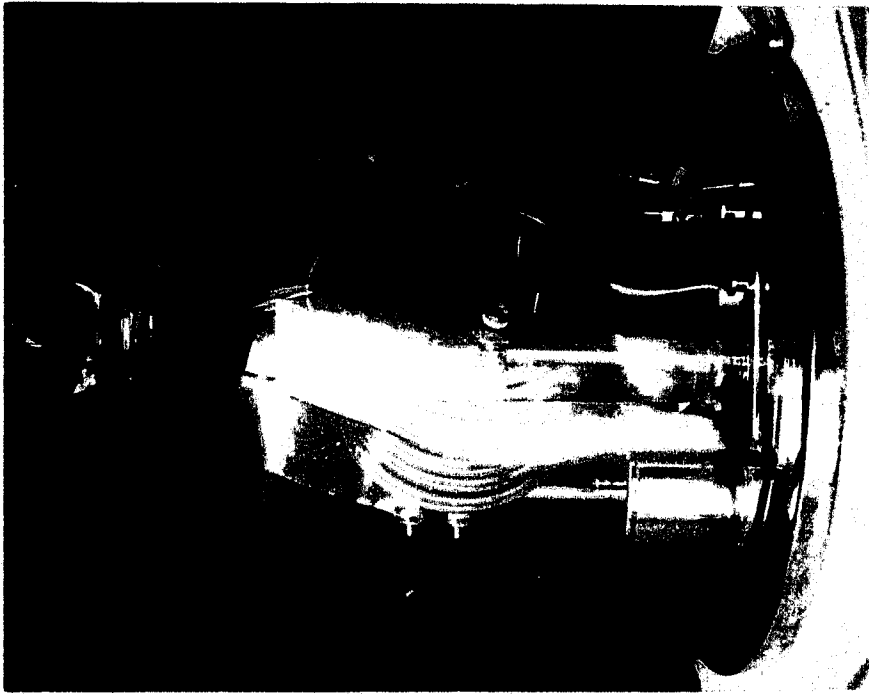


Figure 5(a). JEOLCO evaporator.



**Figure 5(b). Vacuum chamber.
(double exposure)**

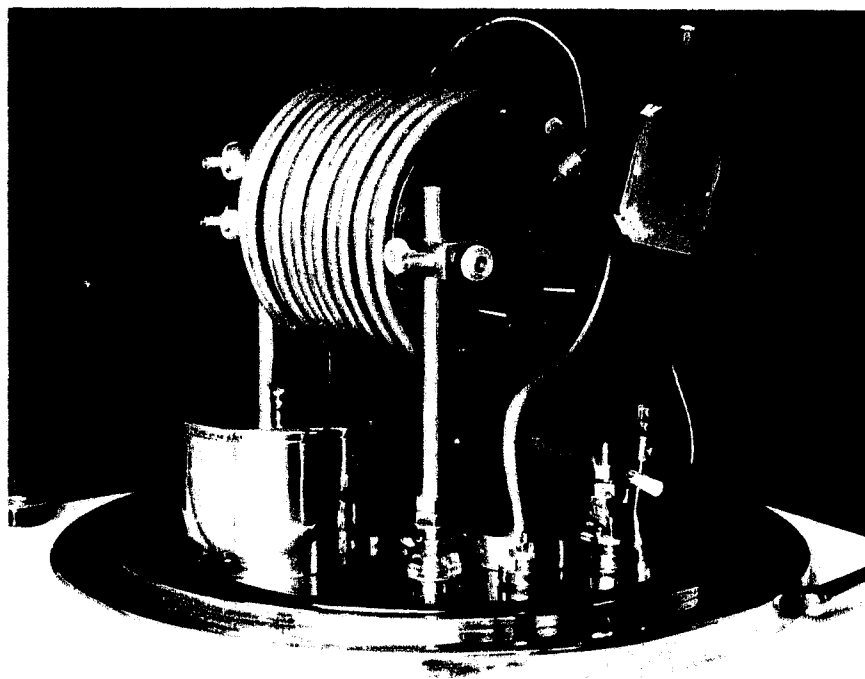


Figure 5(c). Vacuum furnace.

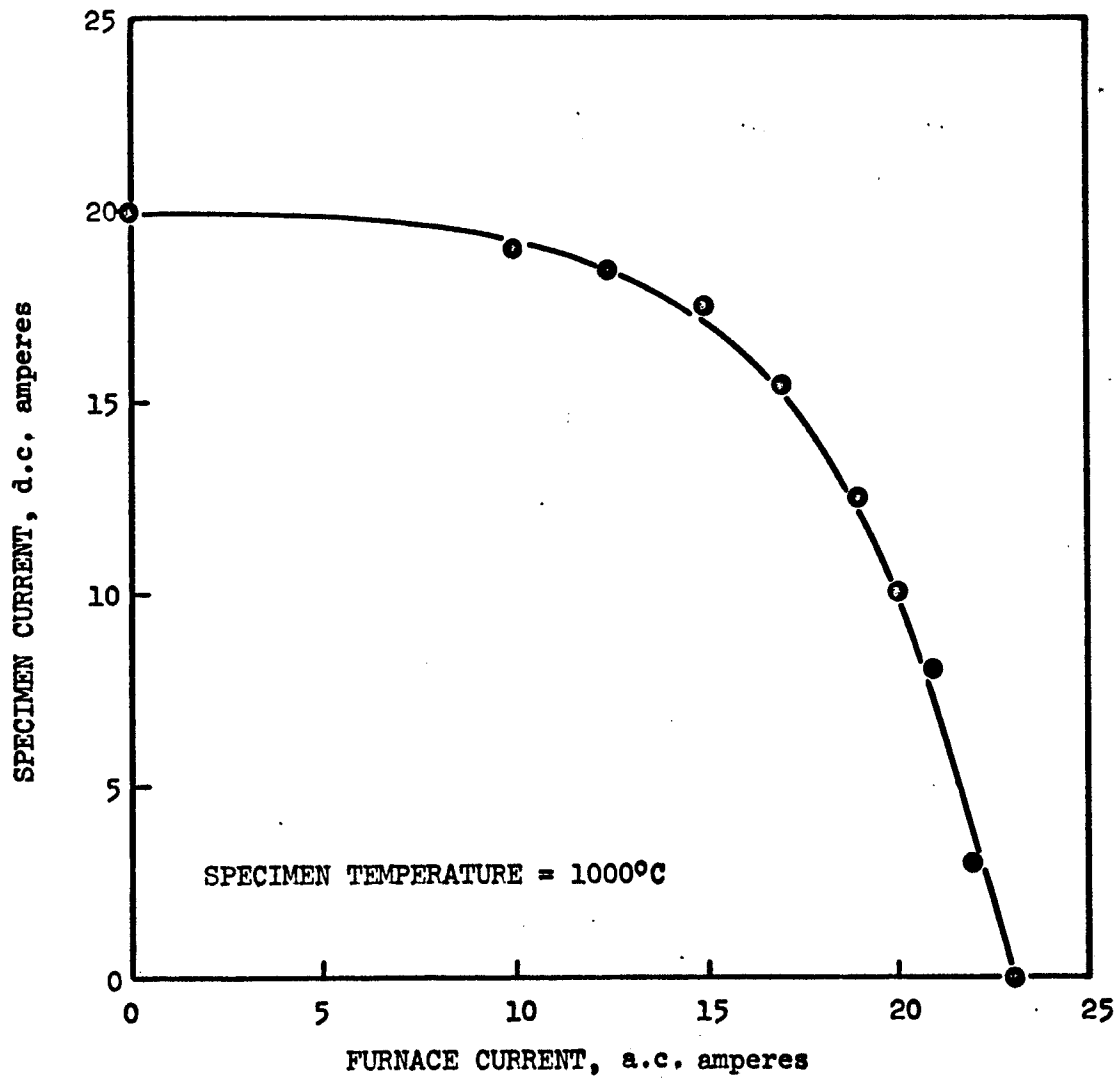


Figure 6. Values of furnace and specimen currents required to maintain a specimen at 1000°C.



Figure 7. Central section of specimen with thermocouple probes spot-welded in position. x 14

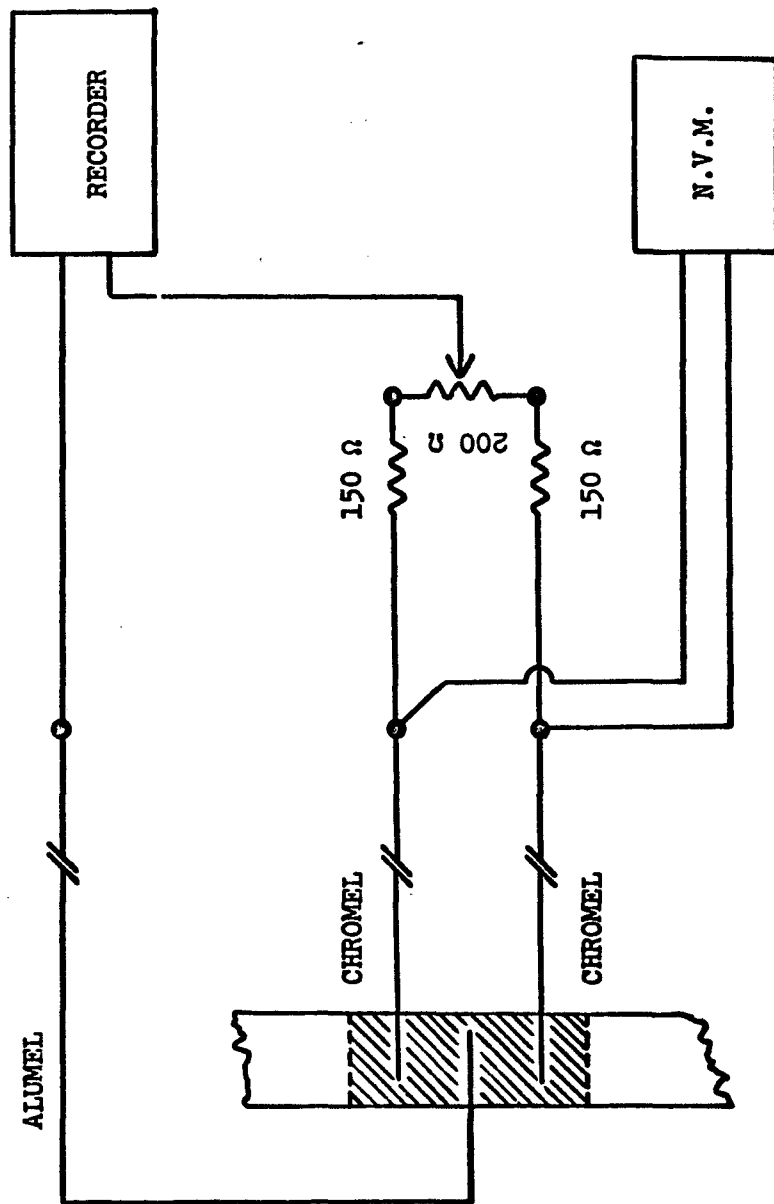


Figure 8. Diagram of measuring circuit.

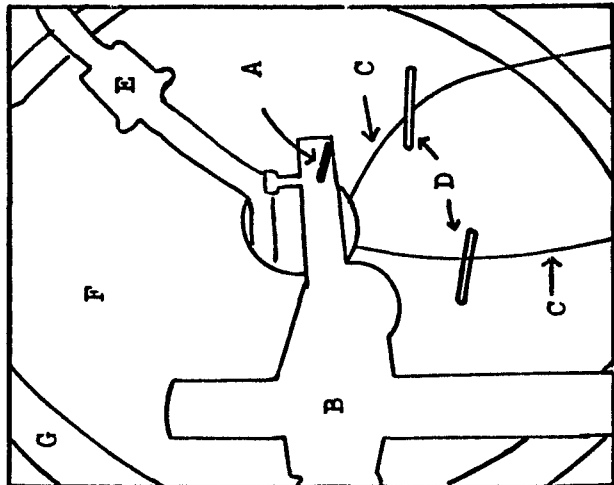
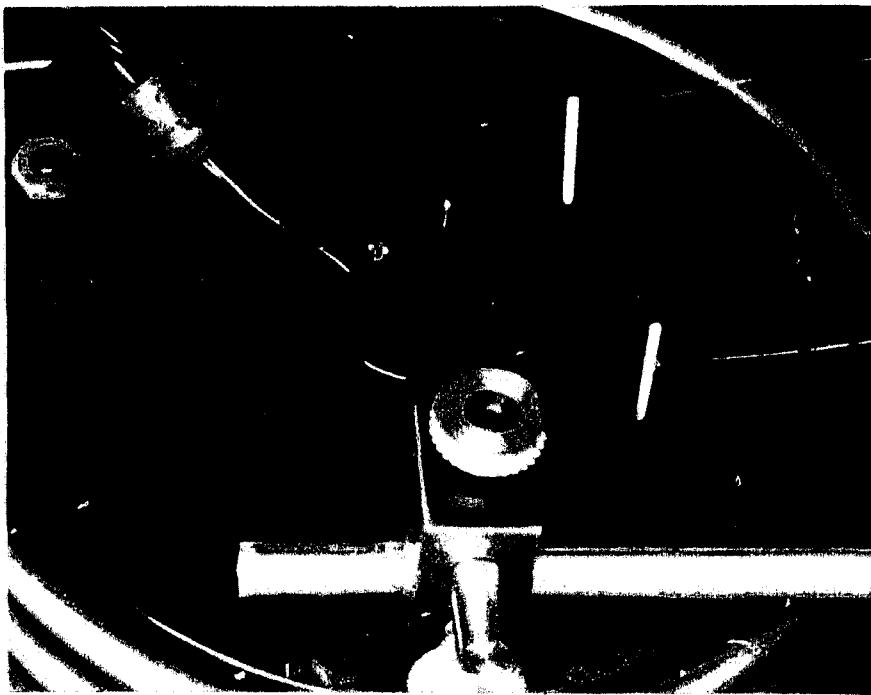
signal fed to a Hewlett Packard D.C. Null Voltmeter (Model 419A) to measure the electric field in the central section of the sample.

The resistances in the balance circuit and the input impedances of the recorder and voltmeter were sufficiently high to insure that only a negligible current flowed in the measuring circuit.

D. ELECTROTRANSPORT RUN PROCEDURE

For electrotransport runs specimens were placed centrally in and axially parallel to the furnace, and were supported by water cooled electrodes as shown in Figure 9. The probes were led out of the furnace to feed-throughs. The natural rigidity of the probes prevented any short circuiting within the specimen chamber.

With the specimen in position the system was closed and evacuated to about 5×10^{-5} Torr. Power was supplied to the furnace until a steady temperature was established. This furnace temperature varied according to the specimen current density and specimen temperature required; for the highest current density tests no power was supplied to the furnace. A direct current was then passed through the specimen and its temperature thus raised (by Joule heating) to the required temperature for the particular experiment. During this heating up period (ranging from 5 to 10 minutes) the applied field was reversed every 30 seconds to minimise electrotransport at intermediate temperatures. The experiment was timed, and a fixed polarity maintained, when the required specimen temperature was reached. The measuring



- A. Specimen.
- B. Specimen Support & Power Lead.
- C. Thermocouple Wires.
- D. Alumina Spacers.
- E. Furnace Power Leads.
- F. End Plate.
- G. Copper Coil.

Figure 9. Close-up of furnace, showing specimen connection to cathode current terminal and thermocouple probes.

circuit was balanced during the heating up period and also when a steady temperature was reached.

The temperature of the specimen was controlled manually, mainly through corrections to the furnace power. After the first 30 minutes very steady conditions prevailed and only a few minor adjustments were required. The balance of the measuring circuit was checked every 30 minutes, but adjustments were seldom necessary. Electrotransport runs usually lasted about 6 hours, although shorter and longer tests were also made. During this time the specimen temperature was continuously recorded; the current density and applied field were read every 30 minutes.

When heated, the specimens tended to buckle slightly due to thermal expansion and stress relief, forming a gentle 'S' curve. The central 3" of the specimens appeared to be at fairly constant temperature, and over the central diffusion region (0.25") it is unlikely that temperature differences greater than 1°C existed. The electrotransport runs were terminated by shutting down the specimen current and the furnace power, and allowing the specimen to cool under vacuum. The accuracy of temperature control and the temperature gradient along the specimen are more fully discussed in a later section concerning error analysis.

E. ANALYSIS

After electrotransport the specimens were marked for polarity and the spacing between the outer chromel probes measured on a microscope. A section of the specimen, measuring about 1"

and including the diffusion zones, was austenised for 10 minutes at 925°C under argon and quenched into iced brine. These specimens were mounted in bakelite, ground to the center of the wire, polished and etched in 2% Nital solution.

Hardness readings were taken on a Leitz Durimet Microhardness Tester at a load of 500 grams. This machine was provided with a moveable stage controlled by micrometers. Microhardness traverses (usually three) were made along the wire in the region of the welds as shown in Figure 10. The positions of the indentations and the welds were obtained from the micrometer scales. Hardness values were converted to carbon concentrations using a calibration curve. A computer program (see Appendix II) was used in this calculation.

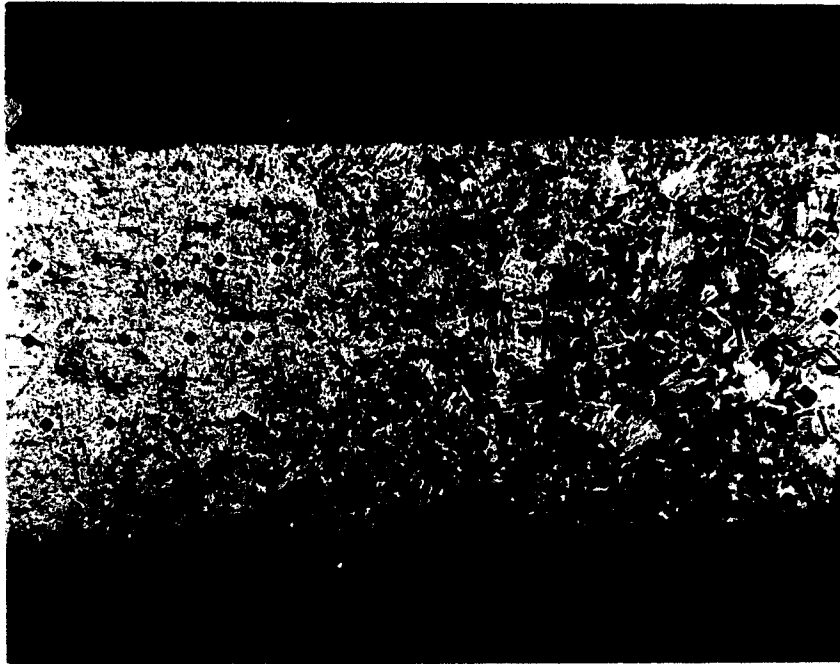


Figure 10. Typical series of hardness indentations straddling a weld. Martensitic structure changes from fine to coarse as carbon concentration diminishes from left to right.
x 60

RESULTS

The calibration of hardness versus carbon concentration for iron-carbon martensite is given in Figure 11. The Metals Handbook²² calibration for 99.9% martensite is also shown. The correlation between the present calibration and that in the Metals Handbook is considered adequate, particularly since the latter values were converted to VPH from Rockwell C values. The relation between hardness and carbon concentration up to about 0.5 wt % may be closely approximated by a straight line; the equation of this line and the computer program used for the calculation are given in Appendix II. Appendix III gives a conversion table for indentation diagonals, hardnesses and concentrations. Errors in carbon concentration measurements (in the Leco Analyser) are considered negligible. The close agreement between measurements on samples of known composition (Table III) indicates that this is a valid assumption.

The carbon penetration profiles after electrotransport are shown in Figures 12-23. For each sample the anode and cathode curves are superimposed (using the weld interface as the origin) to facilitate measurement of the shift due to electrotransport. A simple statistical analysis was used to calculate the centroids and the slopes (near the $C_0/2$ concentration) for each series of points. Details of this calculation are given in Appendix IV. The penetration curves are drawn freehand, using the centroid and slope values as guidelines. The 'shift' or displacement between anode and cathode curves were measured near the $C_0/2$

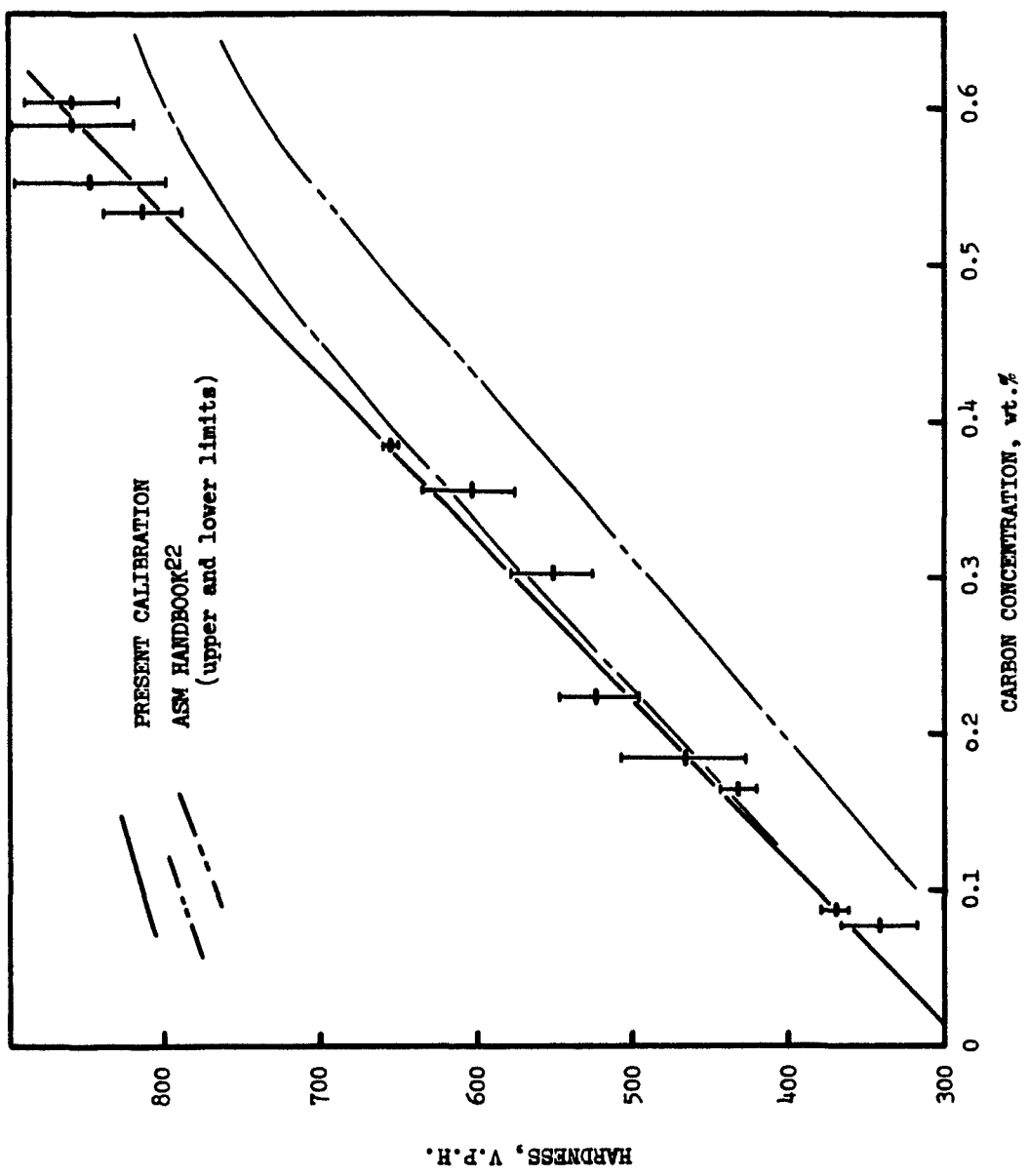
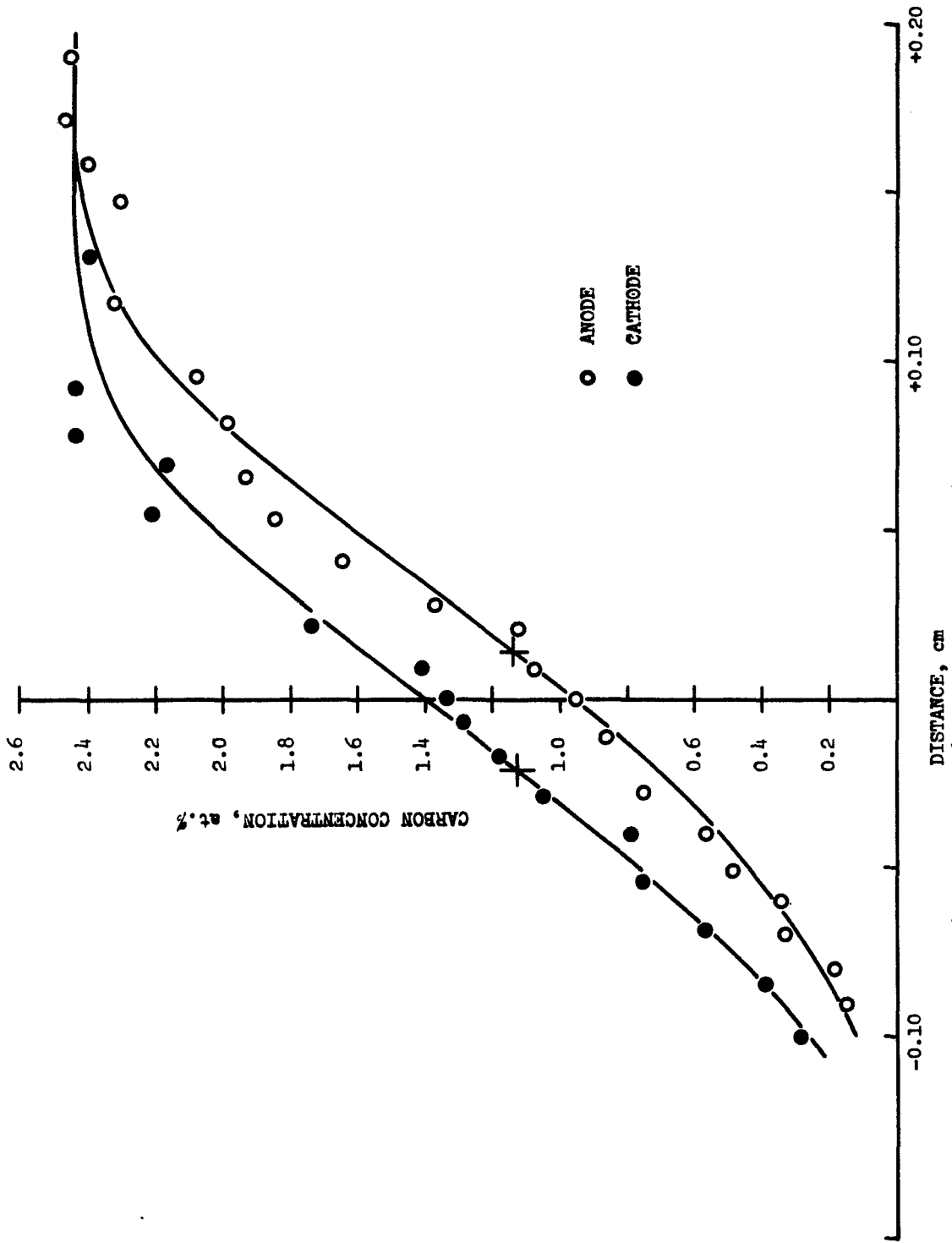


Figure 11. Calibration of hardness against carbon concentration.



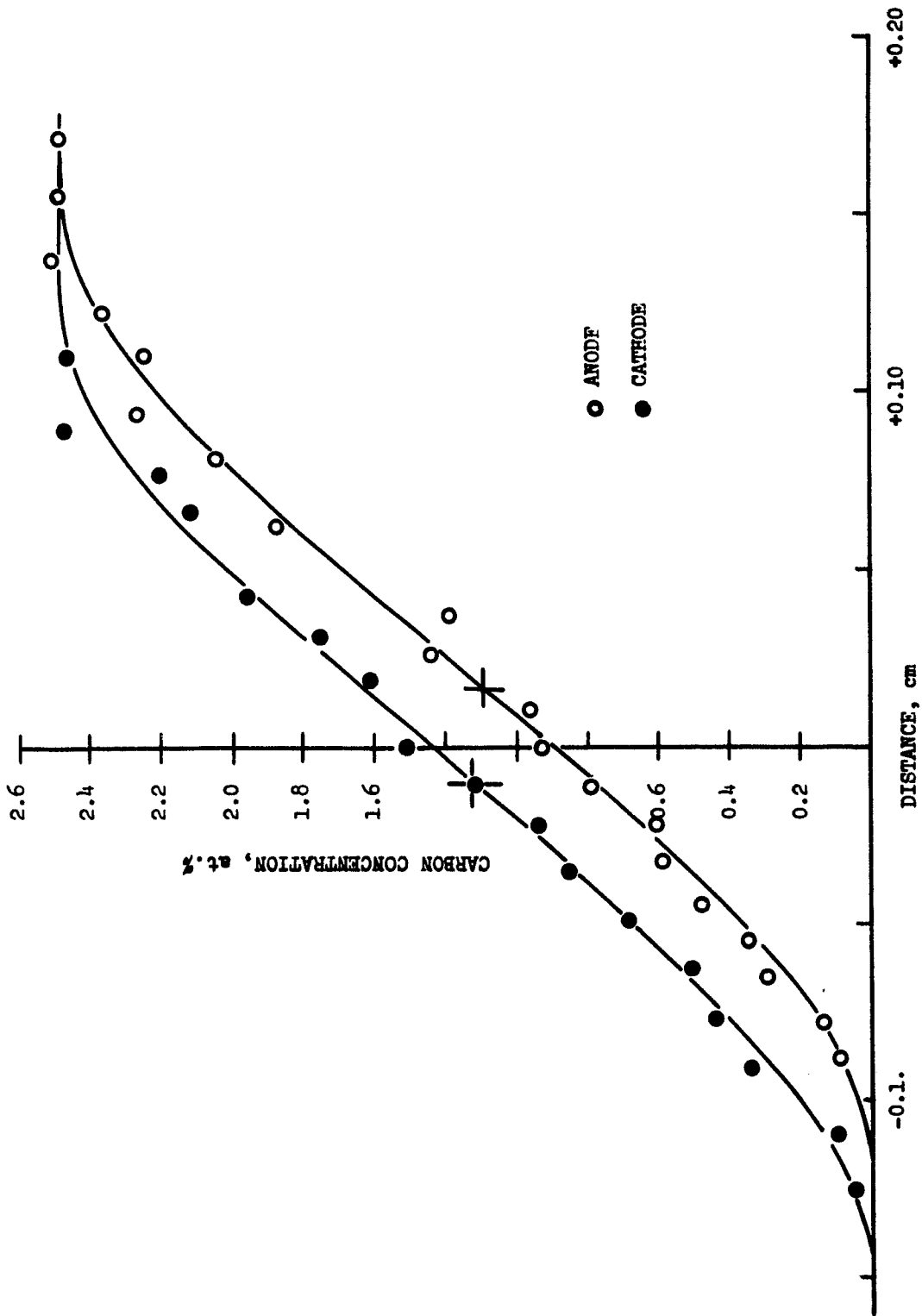


Figure 13. Specimen 13, carbon penetration curves.

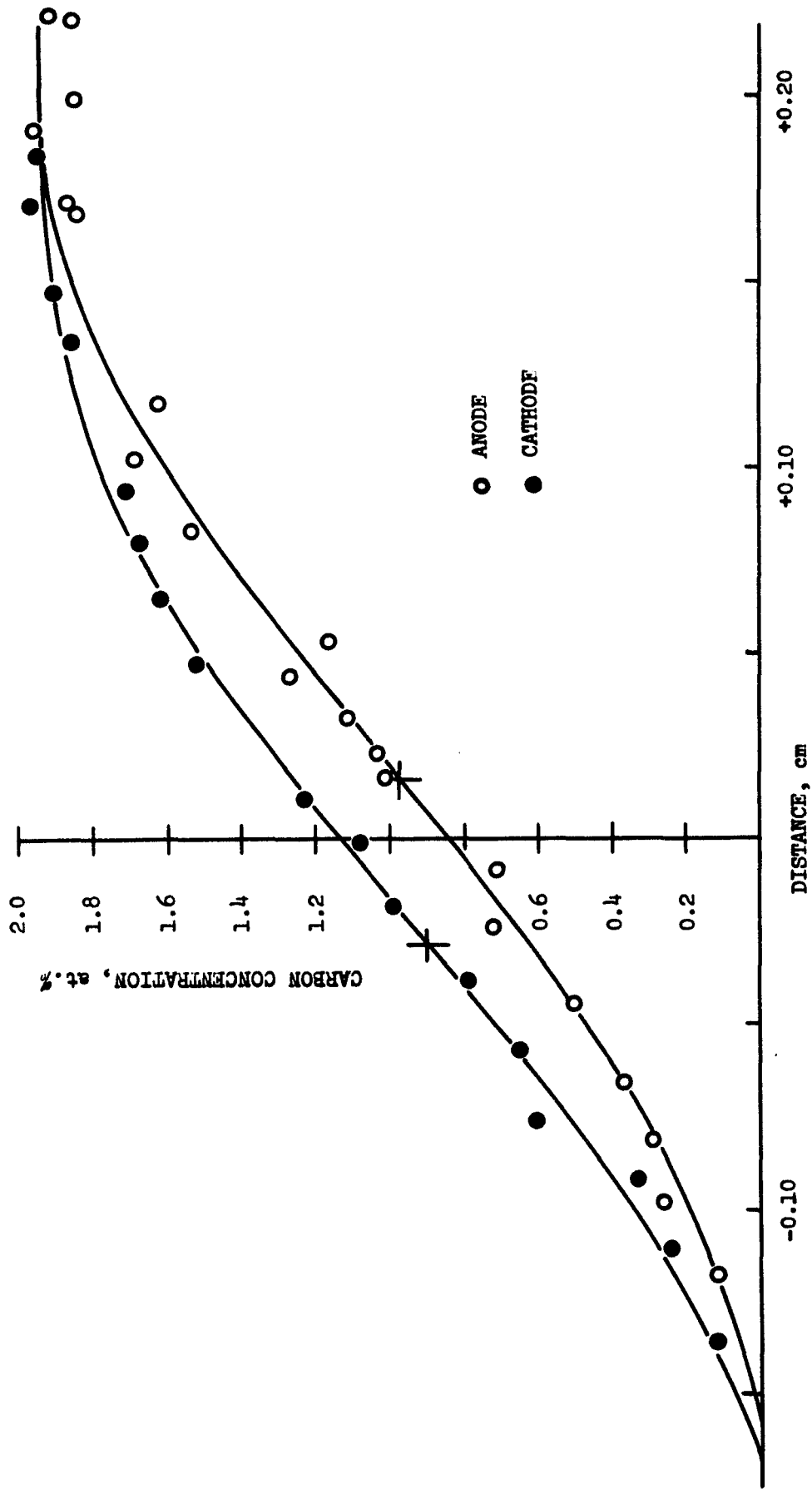


Figure 14. Specimen 14, carbon penetration curves.

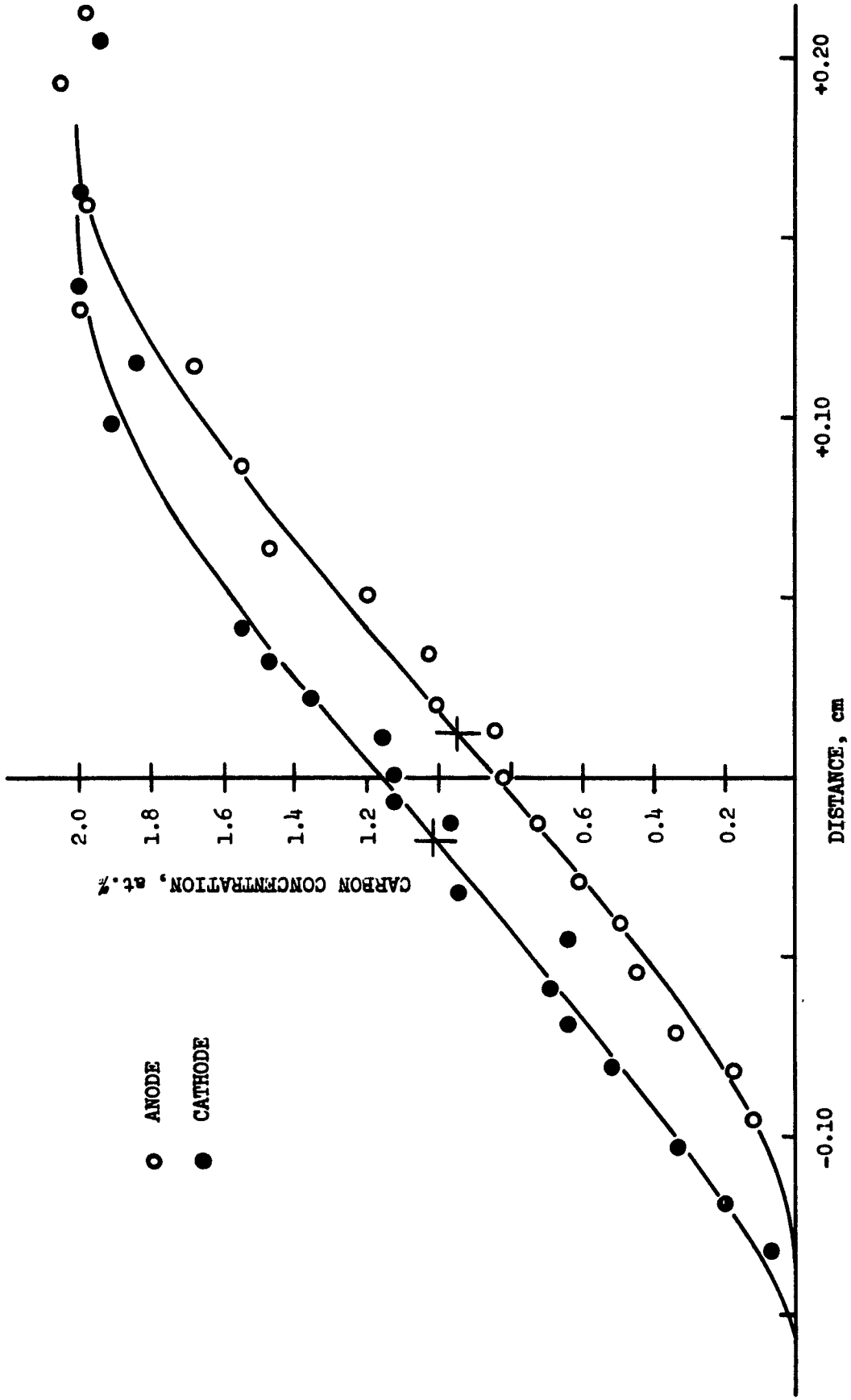


Figure 15. Specimen 10, carbon penetration curves.

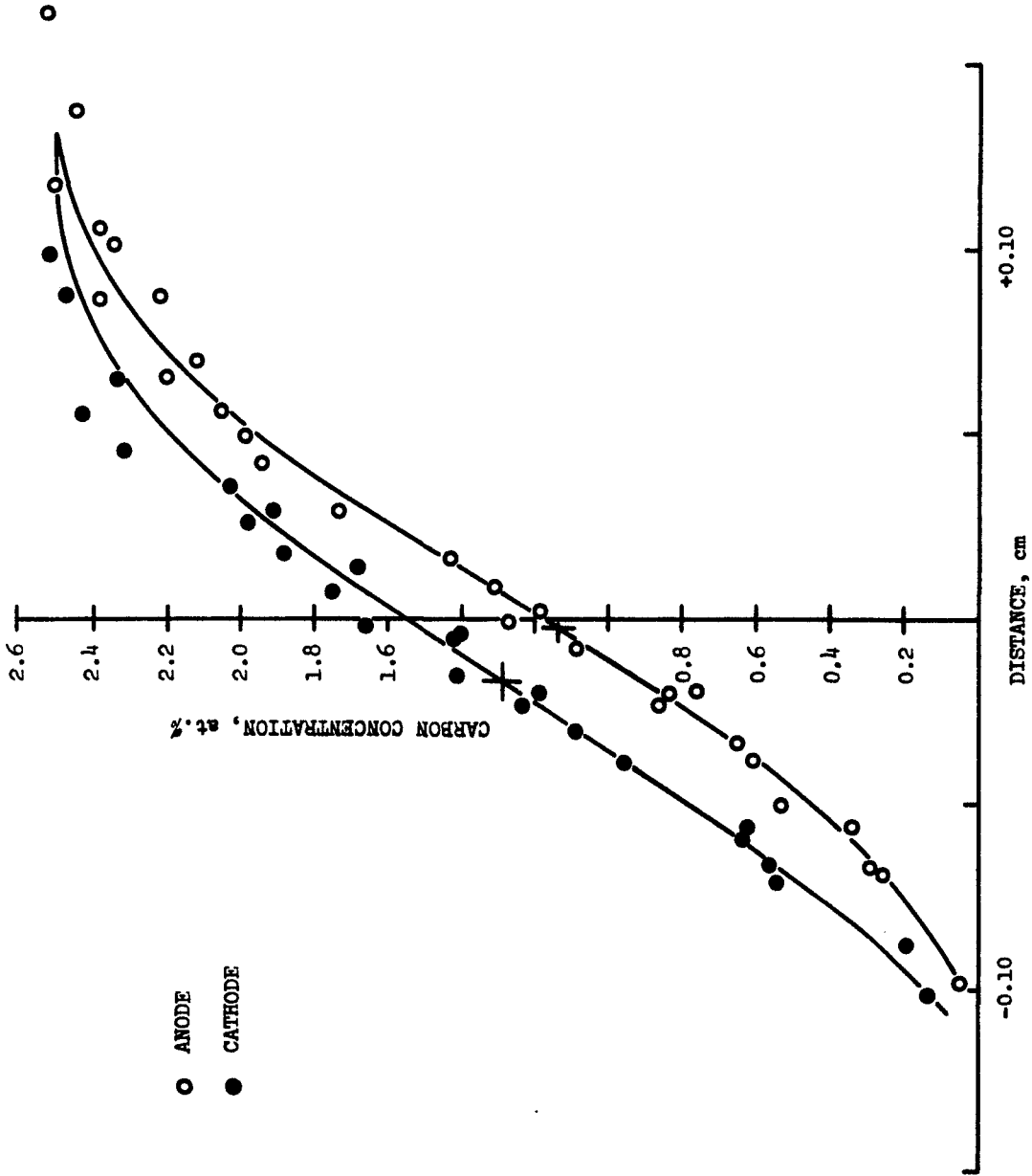


Figure 16. Specimen 19, carbon penetration curves.

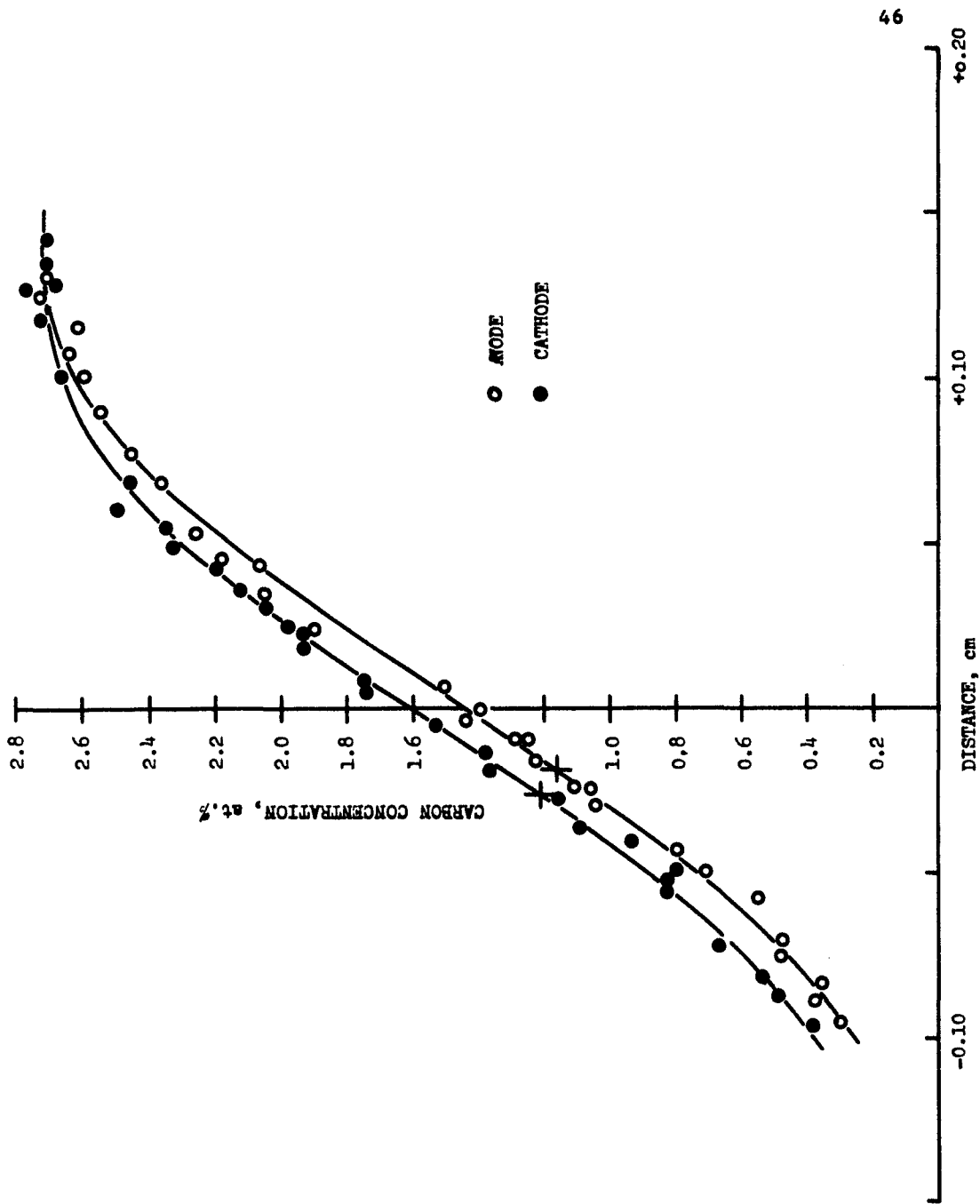


Figure 17. Specimen 20, carbon penetration curves.

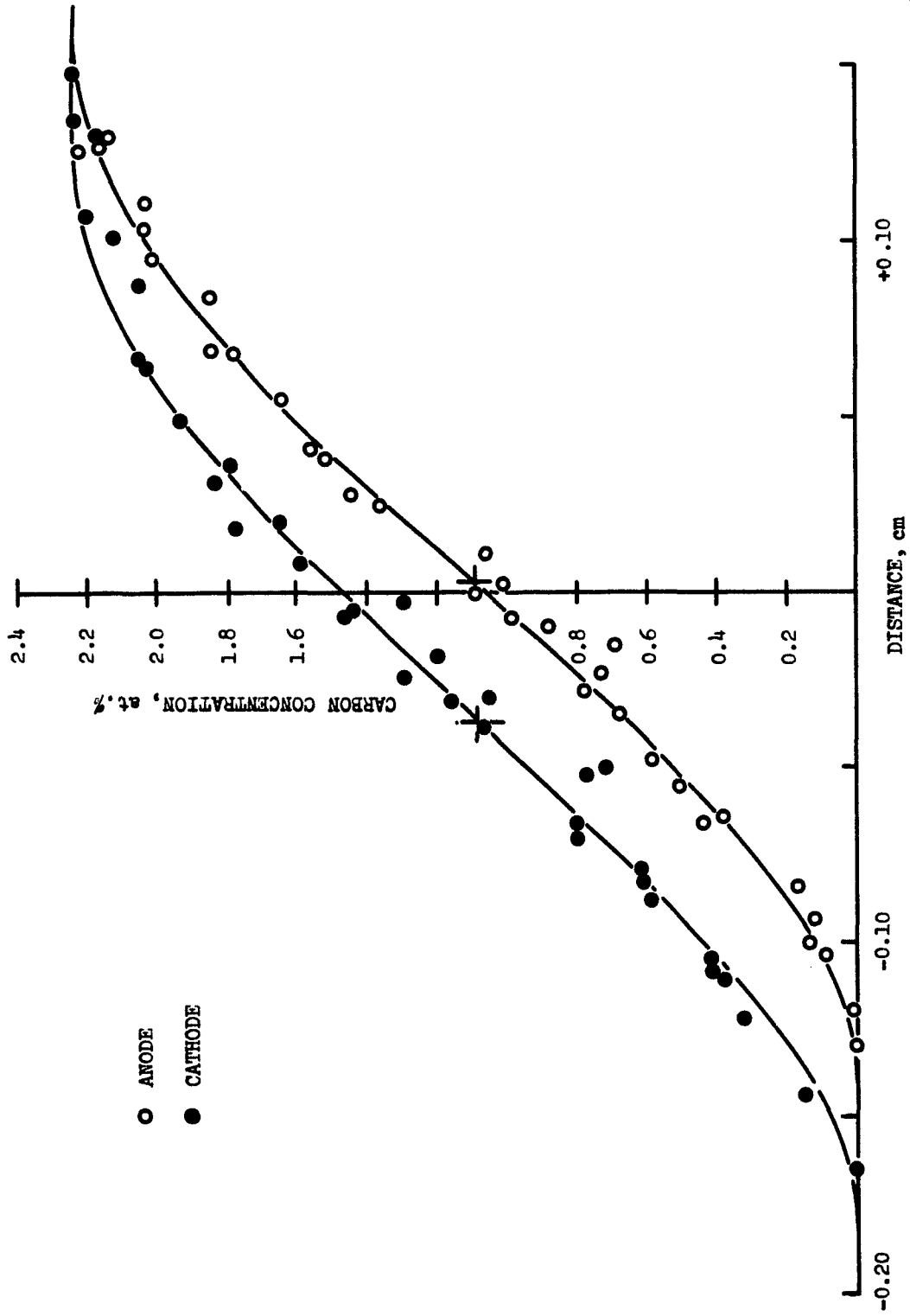


Figure 18. Specimen 22, carbon penetration curves.

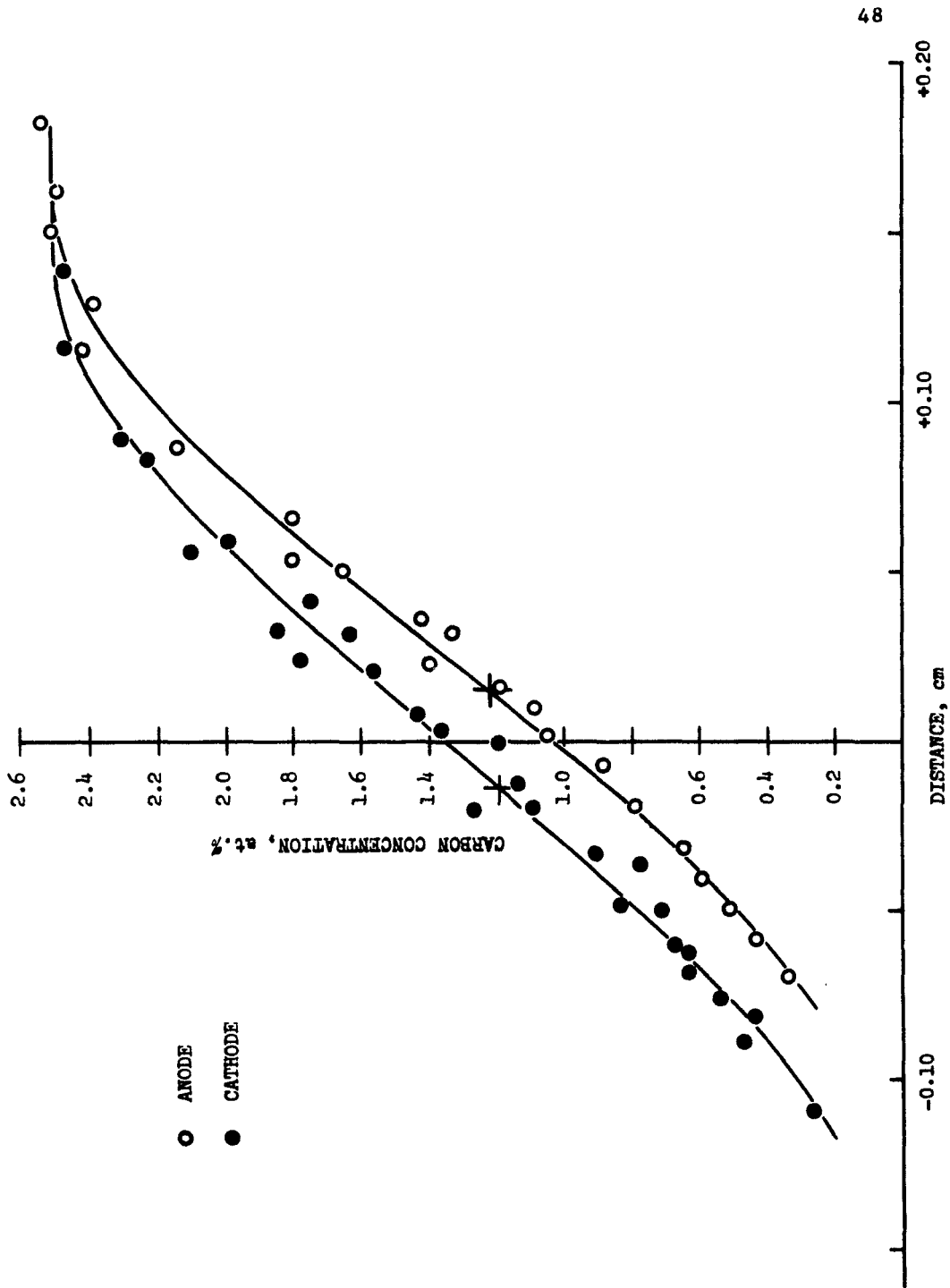


FIGURE 19. Specimen 16, carbon penetration curves.

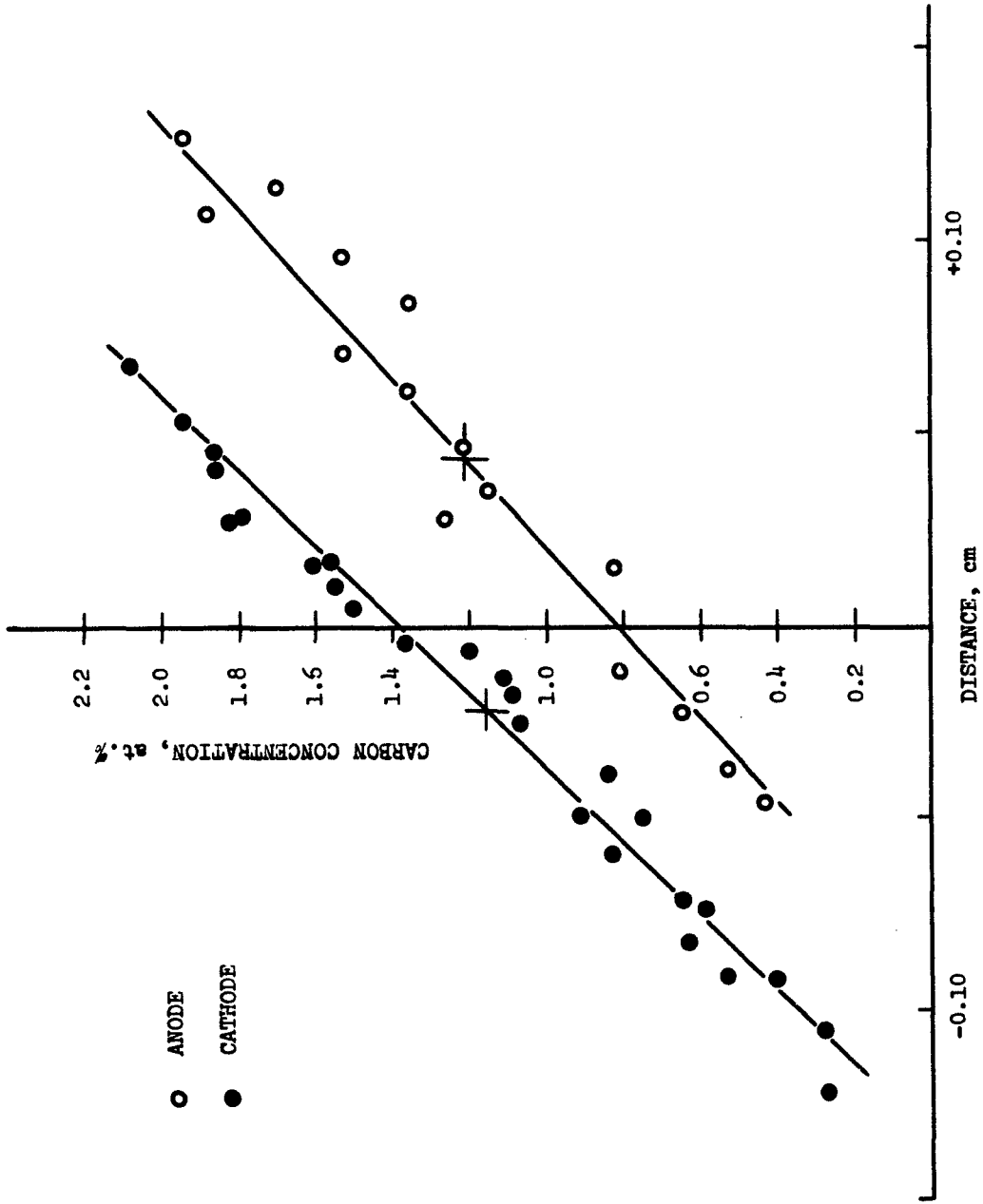


Figure 20. Specimen 17, carbon penetration curves.

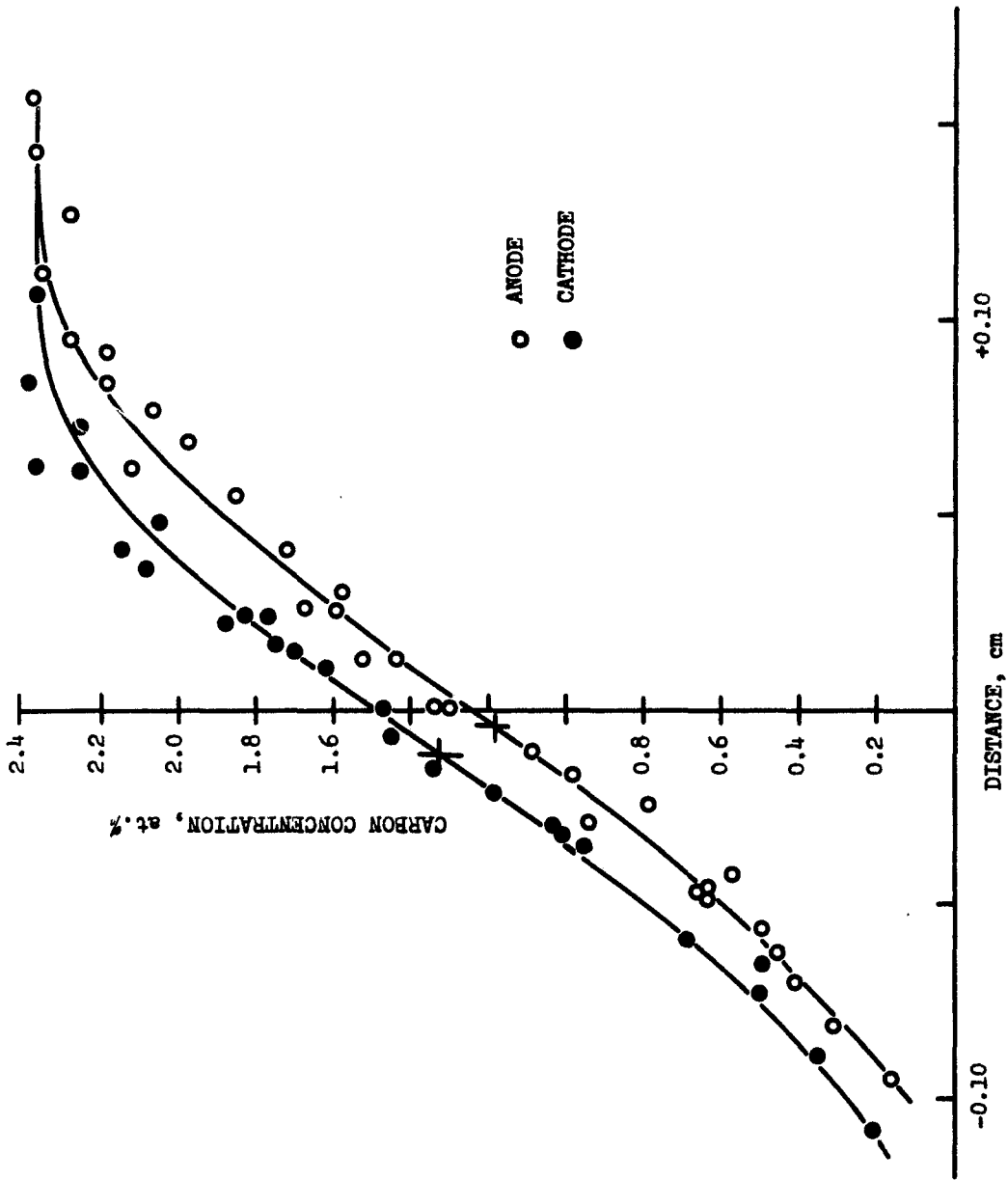


Figure 21. Specimen 18, carbon penetration curves.

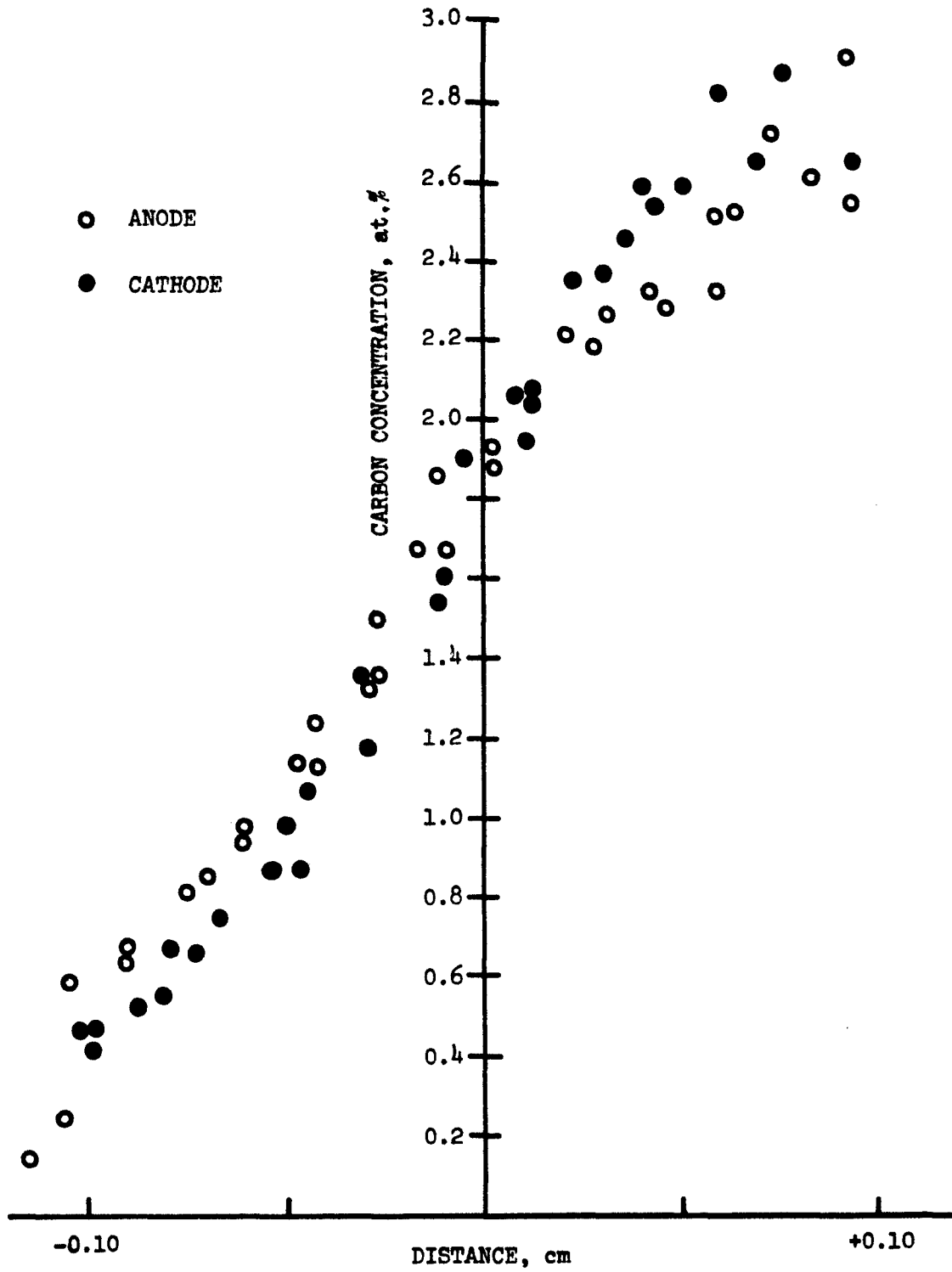


Figure 22. Specimen 24, carbon penetration curves.

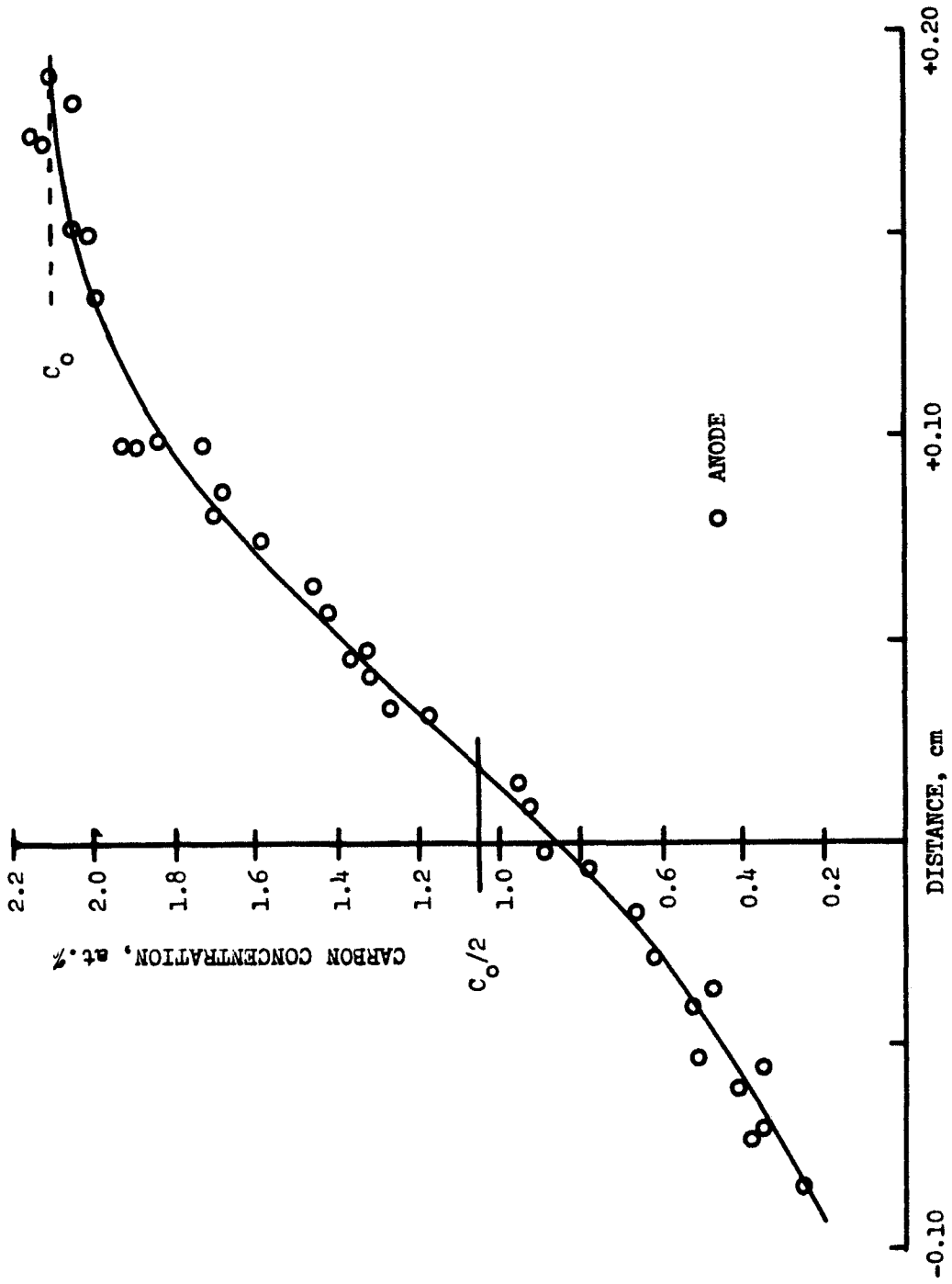


Figure 23. Specimen 25, carbon penetration curves.

concentration. The displacement of carbon due to electrotransport is given by one half the value of the shift (c.f. Equation (9)). A slightly less accurate measurement may be made on a single weld by measuring the distance from the plane of composition $C_0/2$ to the weld interface. This method was employed in sample #25, where one of the welds was found to be unsuitable for analysis.

The experimental conditions for each specimen are summarised in Table IV. Data measured from the penetration curves are shown in Table V. Other calculated results are given in Table VI. The equations used in obtaining these results and a complete sample calculation are shown in Appendix V.

In the calculation of effective charges accurate values of carbon diffusivities are essential. In Figure 24 the diffusivities obtained by different investigators (under conditions comparable to the present experiments) are plotted against the reciprocal of absolute temperature. The diffusivities calculated for the high current density samples (samples #10, #11, and #16), are also plotted, and show good agreement with published data. Low current density samples underwent fairly long anneals at intermediate temperatures due to the slow heating and cooling times of the furnace. The diffusivities calculated for these samples were not considered to be very accurate. Since $\log D$ versus $1/T$ is a straight line the best fit straight line through the points was drawn, and from this the diffusivity values used in the calculations were obtained.

Values of electrical resistivity were also calculated;

TABLE IV

Experimental Conditions

Specimen Code	Temperature °C	Time s $\times 10^{-4}$	Field $\nu \text{ cm}^{-1}$ $\times 10^{+2}$	Current A
11	920	2.53	9.66	9.54
13	920	2.52	6.25	5.97
14	920	3.96	2.84	2.71
10	950	2.34	10.58	9.97
19	950	1.86	4.03	3.82
20	950	2.16	1.94	1.80
22	950	3.24	2.75	2.70
16	980	1.44	11.06	10.52
17	980	3.24	5.08	4.83
18	980	1.50	2.47	2.32
24	980	1.91	1.77	1.60
25	980	2.00	2.81	2.70

TABLE V

Data from Penetration Curves

Specimen Code	Shift cm	Velocity $\text{cm s}^{-1} \times 10^{+7}$	Mean C_o at %	Slope at $C=C_o/2$ at % cm^{-1}
11	0.0340	6.517	2.40	12.96
13	0.0275	5.456	2.21	12.05
14	0.0355	4.480	1.96	7.91
10	0.0370	7.906	2.00	8.71
19	0.0235	6.317	2.71	14.80
20	0.0110	2.550	2.87	15.68
22	0.0390	6.019	2.38	10.93
16	0.0265	9.201	2.44	12.36
17	0.0590	9.105	2.60	9.70
18	0.0170	5.667	2.83	14.40
24	0	0	2.80	16.00
25	0.0340	8.500	2.30	10.60

TABLE VI

Calculated Results

Specimen Code	Effective charge q_{eff}	$1/J^*$ $cm^2 A^{-1}$ $\times 10^{+3}$	Resistivity cm^{-1} $\times 10^{+6}$	Diffusivity $.cm^2 s^{-1}$ $\times 10^{+7}$
11	5.56	1.08	104.33	1.08
13	7.24	1.73	108.13	1.06
14	13.09	3.79	107.64	1.24
10	4.46	1.03	108.97	1.79
19	9.72	2.69	108.41	1.43
20	8.15	5.70	110.58	1.24
22	13.61	3.80	104.50	1.16
16	3.92	0.98	108.39	2.15
17	8.46	2.13	108.21	1.73
18	10.83	4.42	109.17	2.04
24	0	6.41	113.20	-
25	14.26	3.80	106.85	1.87

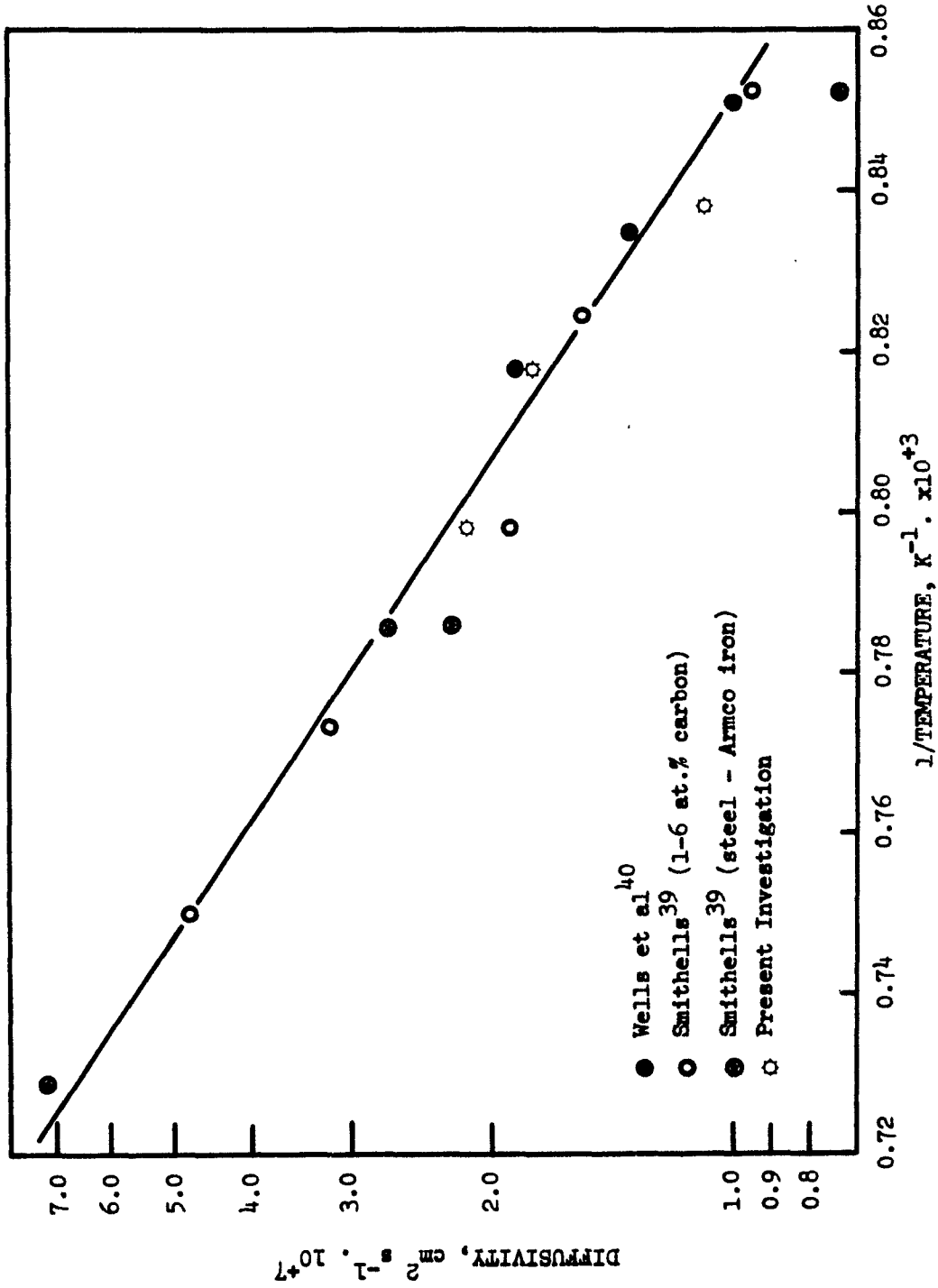


Figure 24. Diffusivity of carbon in iron as a function of temperature.

the mean values for each temperature are given in Figure 25. These results are in fair agreement with results calculated from data in Smithells Metal Reference Book³⁹.

The effective charge values for each temperature investigated are plotted against the reciprocal of current density in Figure 26. This graph shows a pronounced increase in q_{eff} as $1/J$ increases, the relationship being approximately linear; beyond the point $1/J = 4 \times 10^{-3} \text{ cm}^2 \text{ A}^{-1}$ there is a sharp drop in the effective charge. The effect of temperature on the overall effective charge is not marked, though at high current densities the charge values tend to fall as the temperature increases, and this trend is reversed at higher current densities.

Samples #12, #15, #21 and #23 exhibited very poor welds and were not analysed.

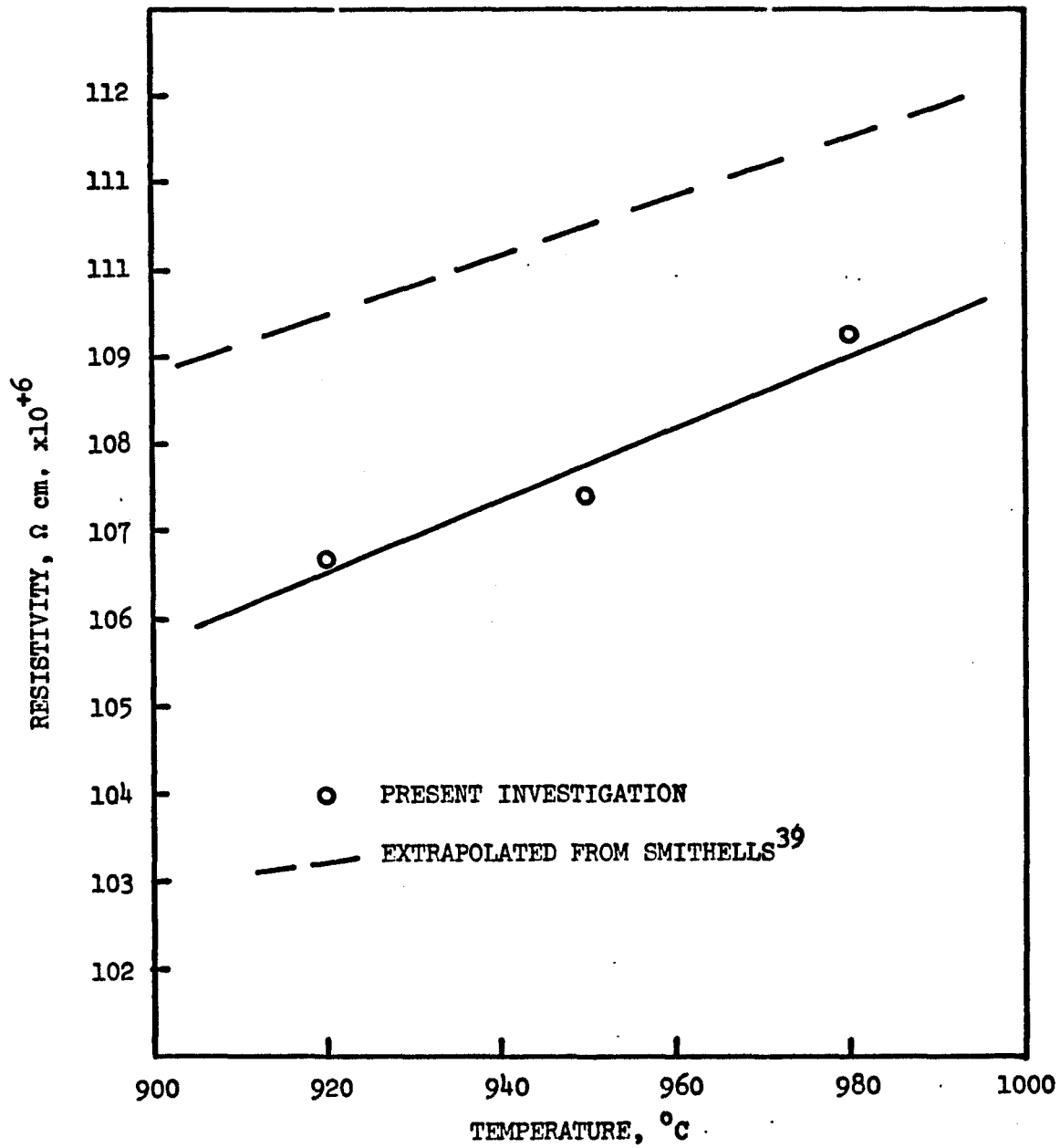


Figure 25. Temperature dependence of the resistivity of iron.

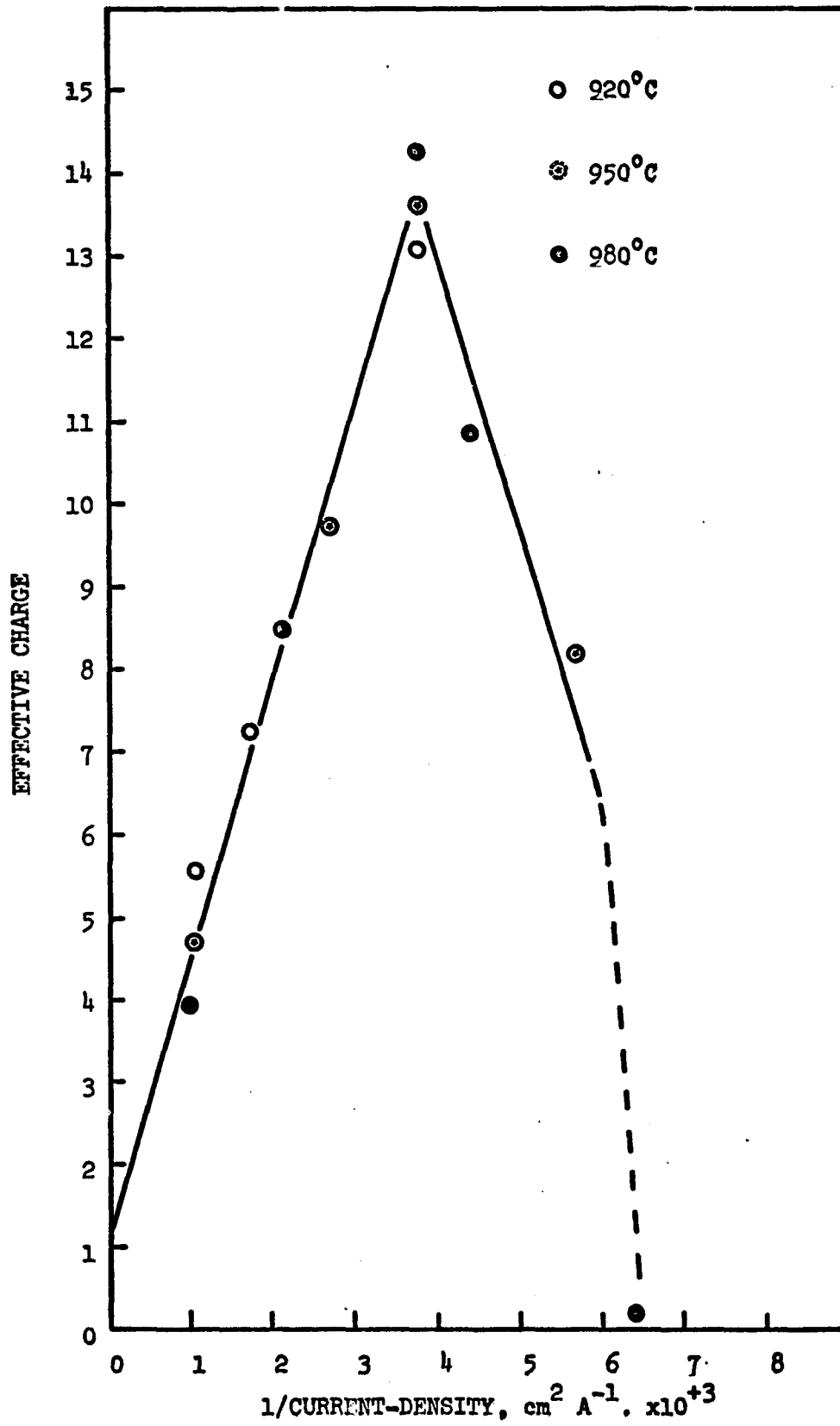


Figure 26. Effective charge values as a function of current density.

DISCUSSION OF ERRORS

Assessing the error implicit in a value calculated from several experimental parameters is seldom a simple procedure. Where a large number of experimental results are available it is only necessary to study the sources of systematic errors, since all random errors may be assessed collectively in a statistical treatment of the data. Where a statistical treatment is not possible it becomes necessary to consider all sources of error and their effect on the accuracy of the final result.

A. ERRORS IN TEMPERATURE AND DIFFUSIVITY

1. Temperature Measurement

During electrotransport runs the specimens were placed symmetrically in the furnace with the carburised section at the exact center of the furnace. The variation in temperature along the central section of the specimen (shown in Figure 27) is about 3°C , but it is unlikely that the mean temperature measured by the thermocouple probes differed by more than 2°C from the mean temperature in the region within the welds. In these measurements a specimen was heated in the furnace to a temperature of 770°C in air. The specimen could be moved along the furnace in order to reposition the measuring thermocouple. It would have been desirable to repeat this experiment under vacuum and at 950°C , both under furnace and specimen (Joule) heating, but this was not readily feasible with the existing apparatus.

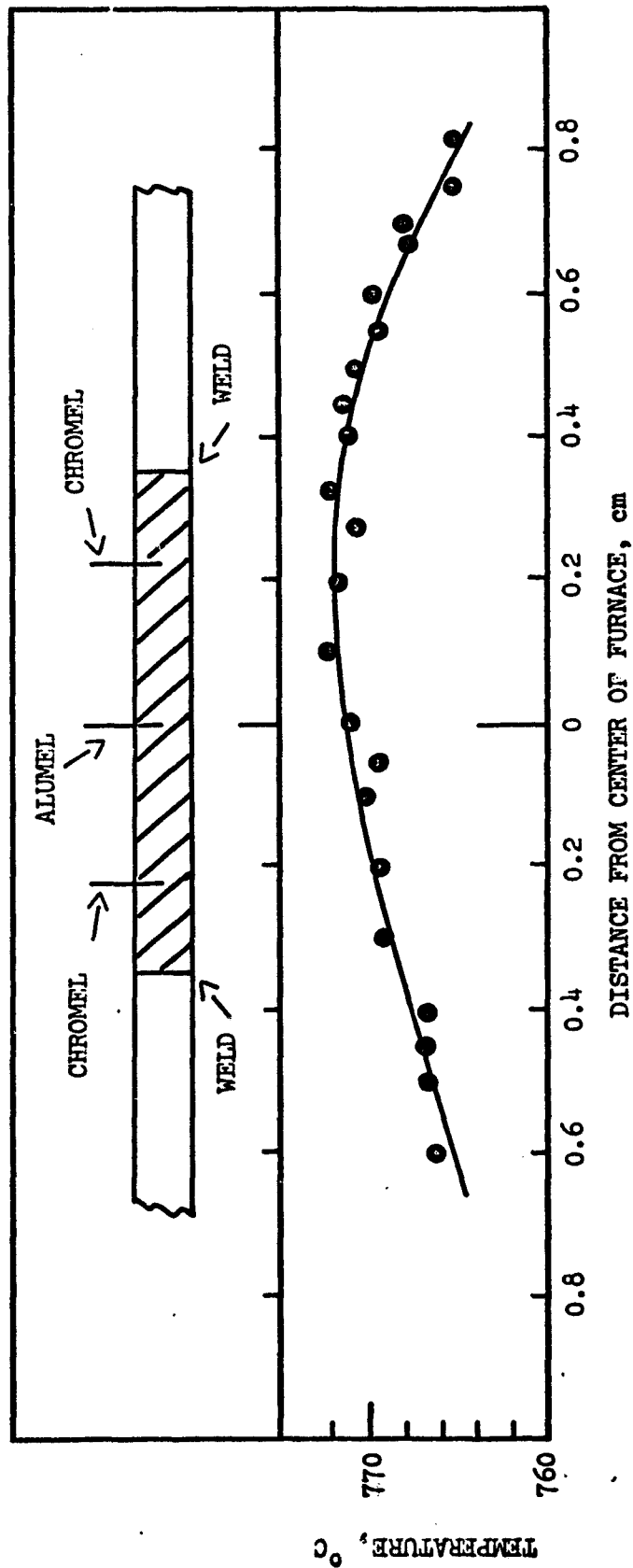


Figure 27. Specimen location and specimen temperature gradient relative to the furnace center.

Instead the voltage drops in the center of the alloy region (ΔV_a) and across a weld ($\Delta V'_a$) were measured and plotted against current as shown in Figure 28. The linearity of the plots indicates that the relative resistivities (and thus the temperatures) of the alloy and weld regions did not change over a wide range of specimen and furnace current combinations, the specimen temperature being maintained at 950°C . The resistivities of the alloy section and across the weld were calculated to be 100.9×10^{-6} ohm cm and 101.5×10^{-6} ohm cm respectively. This difference is probably not significant since the reading error in locating the measuring probe positions (equivalent to about one half the probe width) is about 1%. However, if any credence were to be given to the resistivity difference it would seem that the weld area was 15°C hotter than the central region. This is highly unlikely. Thus, lacking evidence to the contrary, it is concluded that the temperature gradient errors under experimental conditions were probably of the same order of magnitude as those estimates from the measured temperature profile at 770°C .

The probes did not appear to suffer from any contamination which might have caused discrepant temperature measurements. Under vacuum or slightly oxidising atmospheres chromel-alumel thermocouples are fairly dependable, particularly when prolonged use is aided by using new probes for each specimen. However, even in high quality thermocouple wires small errors arise due to inhomogeneities of composition and high temperature annealing during use. Such errors could be as high as $\pm 3^\circ\text{C}$ if they are

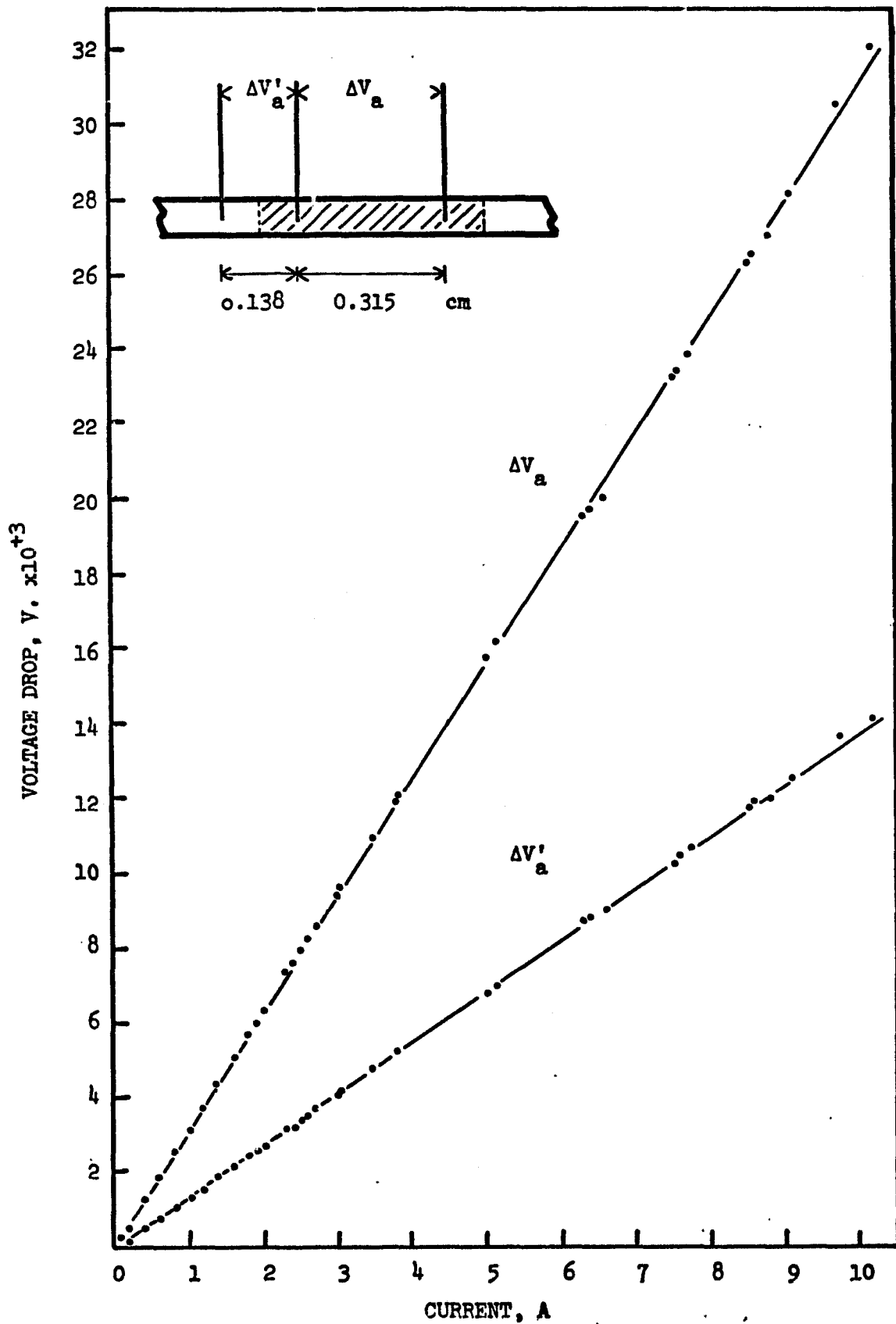


Figure 28. Voltage drops across alloy (ΔV_a) and weld ($\Delta V'_a$) regions versus current at 950°C.

additive, and are usually systematic where wire from the same spool is used under identical conditions in different experiments.

The measuring instruments (recorder, potentiometer and null voltmeter) had sufficiently high input impedances to reduce the current in the measuring circuit to negligible proportions. A current of about 10^{-4} A could flow through the chromel \rightarrow balance resistance \rightarrow chromel loop. In exiting the furnace the probes touched lightly against the lip of the quartz furnace tube. The resistance across two points along the rim of the tube was measured at 2.5 mega-ohms, so short circuiting is considered negligible.

Extraneous thermoelectric voltages were minimised by using chromel and alumel wiring throughout and placing the balance circuit inside a steel container so that all resistances and connections were kept at a uniform room temperature. Nickel plated feed-throughs were used to carry electrical signals through the base plate. These were water cooled (on the outer connection), and it was anticipated that a temperature gradient might develop between the inner and outer terminals giving rise to an extraneous thermoelectric voltage. This possibility was tested by forming a chromel \rightarrow feed-through \rightarrow chromel loop (using a temporary rubber seal) as shown in Figure 29, and measuring the voltage developed during normal furnace operation. A similar test (omitting the balance circuit) was carried out for alumel. Under steady state conditions with the furnace temperature at about 900°C extraneous voltages totalled -37

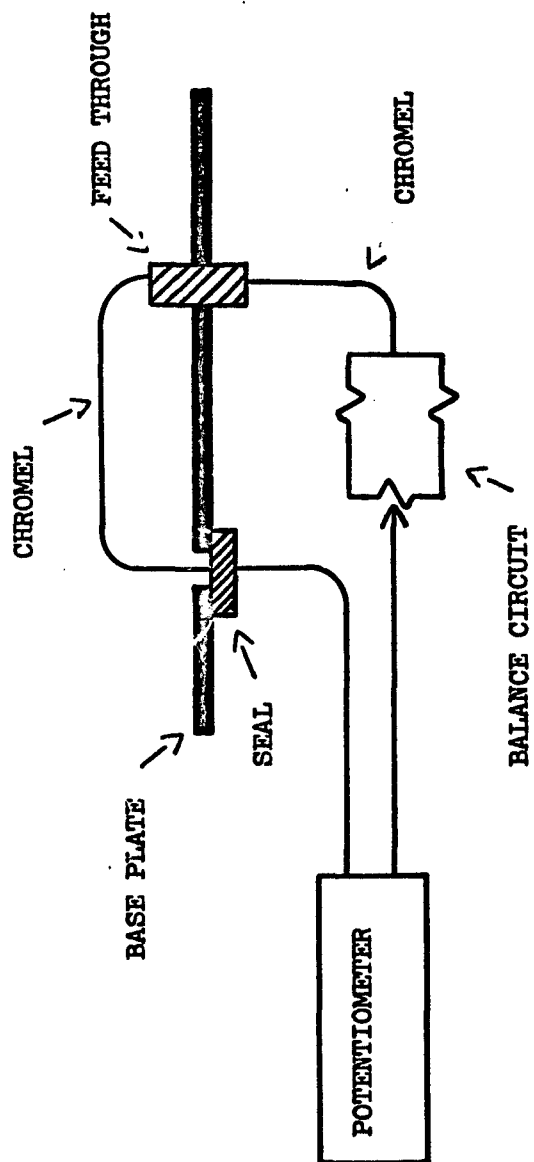


Figure 29. Electrical circuit used to measure thermoelectric effects generated at feedthroughs.

micro-volts, corresponding to an error of less than -1°C .*

The specimen temperature was measured with a recorder and occasionally checked on a potentiometer. Frequent calibration of the recorder insured that the instrument error was contained within the reading error of about $\pm 0.5^{\circ}\text{C}$.

Errors could also arise from irregularities in the a.c. voltage input and an improperly balanced circuit. It was possible for the specimen temperature to drift by as much as 3°C over a period of 30 minutes. Drift errors, which were minimised by frequent checks, were of a random nature and to a large extent self compensating. It is considered unlikely that the net error from this source could have been larger than 1.5°C .

Summing the errors from all sources it may be concluded that the maximum systematic error falls within the limits $+3^{\circ}\text{C}$ ($+0.3\%$) and the random errors probably amount to $\pm 2^{\circ}\text{C}$ ($\pm 0.2\%$).

2. Diffusivity

The diffusivity values used in the calculations were mean values obtained from data in the literature and the results of the present investigation, as shown in Figure 24. The variance of the points about the line in the region 920 to 980°C is about $\pm 0.04 \times 10^{-7} \text{ cm}^2\text{s}^{-1}$, whereas the variance of the mean (i.e. the line) is about $\pm 0.005 \times 10^{-7} \text{ cm}^2\text{s}^{-1}$. It is probably safe to assume that the systematic error in the selection of D values is no larger than $\pm 0.01 \times 10^{-7} \text{ cm}^2\text{s}^{-1}$.

A larger error in D arises as a consequence of the error in

* Where possible the signs of errors are reported. Negative errors occur when the true value is less than the measure value.

temperature. Over the range in question a change of 1°C in T produces a change in D of $0.015 \times 10^{-7} \text{ cm}^2 \text{ s}^{-1}$. Thus the total random error in D was calculated to be $\pm 0.03 \times 10^{-7} \text{ cm}^2 \text{ s}^{-1}$ ($\pm 2\%$), the limits of systematic error being $\begin{matrix} +0.06 \\ -0.10 \end{matrix} \times 10^{-7} \text{ cm}^2 \text{ s}^{-1}$ ($\begin{matrix} +3 \\ -5 \end{matrix} \%$).

B. ERRORS IN ELECTRICAL MEASUREMENTS

1. Electric Field

In high current density experiments the applied voltage (over the central region) was measured with great precision, but in the course of the run a slight instability or drift could occur. In low current density experiments the errors due to voltage drift were extremely small but the reading error became significant. An overall voltage error of about $\pm 4\%$ is considered possible. A further error of $\pm 1\%$ in the measurement of the interprobe separation brings the total random error in electric field measurement to a maximum of $\pm 5\%$.

2. Current Density

Sources of error in current density measurements were analogous to those in electric field measurement, viz. current drift, reading error and wire cross sectional area. The total maximum random error is estimated at about $\pm 2\%$.

3. Resistivity

If in the calculation of resistivities the errors in electric field (E) and current density (J) are considered to be additive then a maximum total error of $\pm 7\%$ is arrived at.

However, the standard deviations in resistivity measurements at a given temperature is about 3%. This probable error of $\pm 3\%$ is considered to be in reasonable agreement with the calculated maximum error of $\pm 7\%$. Thus, considering the probable errors in electrical measurements to be about one half the maximum errors, the probable errors in E and J may be estimated to be about 2% and 1% respectively.

The mean values of resistivities differ by about 3% from the values in the literature. This could be construed as a systematic error, but an exact value cannot be estimated since the data in the literature are also subject to some error. The systematic errors in E and J are estimated to be no larger than $\pm 3\%$.

C. ERRORS IN POSITION OF CONCENTRATION PROFILES

1. Calibration Curve

The calibration curve of hardness against concentration is considered to be sufficiently accurate for the present experiments. It must be noted that the electrotransport shift may be measured accurately even if the calibration is not known exactly; it is only necessary to establish that in the region of interest the concentration is a monotonic function of hardness.

An inaccurate calibration could result in errors in the measurement of diffusivities. However, the close agreement between the calculated diffusivities and the data in the literature verifies the accuracy of the calibration.

2. Heat Treatment

Hutchinson⁴¹ has shown that variations in the austenising temperature, soaking time and quenching rate (above a minimum value) produced negligible changes in the hardness of iron-carbon martensite. Nevertheless all specimens were subjected to identical austenising and quenching conditions.

Microhardness analysis on samples before and after high temperature annealing in the vacuum furnace indicated that decarburisation was negligible. This is also shown by the homogeneity of the structure in Figure 4(b), and the agreement between hardness readings taken across the width of the sample. Figure 4(b) does however, indicate a decarburised region near the edge of the specimen. This decarburisation occurred during austenising and quenching, and this region was avoided in the microhardness analysis.

It should be emphasised that any unsuspected errors in heat treatment or decarburisation are unlikely to affect the accuracy of electrotransport velocities, since in any one sample both welds are subjected to identical conditions.

3. Temperature Gradients

Temperature gradients have already been discussed with reference to errors in temperature and diffusivity. A temperature difference between two welds in ordinary diffusion would give rise to differently shaped penetration curves, but would cause no change in the position of the plane of composition $C_0/2$. In electrotransport a different situation arises. Where both welds are at a temperature T both penetration curves are displaced

from the welds by a distance d , as shown in Figure 30, giving a shift $2d$. Consider a sample at a mean temperature T , with the anode at $T - \Delta T_a$ and the cathode at $T + \Delta T_c$. Under these conditions the anode curve is displaced by $d - \Delta d_a$ and the cathode curve by $d + \Delta d_c$, due to the difference in diffusivities.

Hence:

$$\begin{aligned} \text{SHIFT} &= (d - \Delta d_a) + (d + \Delta d_c) \\ &= 2d - (\Delta d_a - \Delta d_c). \end{aligned}$$

If $\Delta T_a \approx \Delta T_c \ll T$,

then $\Delta d_a \approx \Delta d_c$

Therefore $\text{SHIFT} \approx 2d$

Thus for small temperature gradients very little error in shift is produced; for a gradient of 2°C between the probes the error is less than 0.1%.

4. Location of Welds

Weld interfaces were usually located with great accuracy; however, where slightly curved interfaces or interfaces not exactly parallel to the wire axis occurred some slight uncertainty in the weld location resulted. It is estimated that this contributed a maximum of 3% error in the shift measurement.

5. Drawing Penetration Curves

Assuming that the indentation positions were essentially free from error, the standard deviation in concentration for a typical curve (specimen #10) was found to be 0.05 at.%. The variance of the mean value, which is the significant error in the position of the centroid, is about 0.01 at.%. In terms of

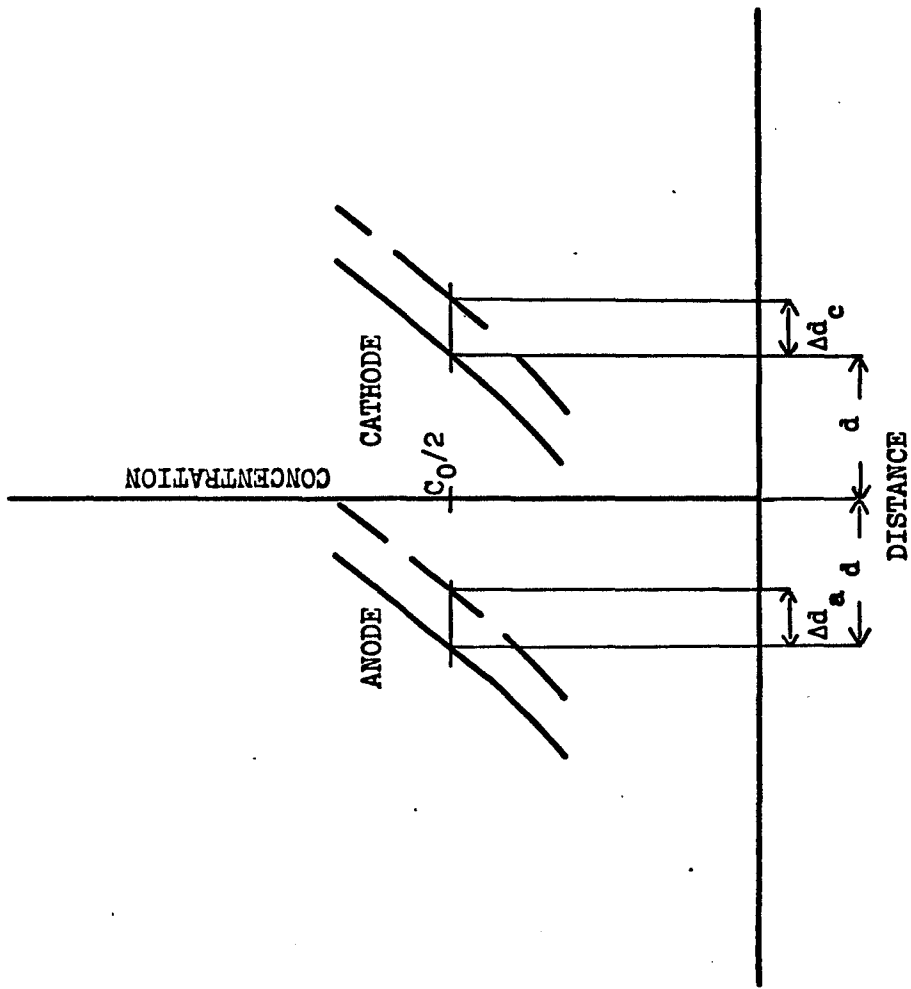


Figure 30. Displacement of penetration curves under electro-transport. Full line: welds at identical temperatures. Broken line: welds at dissimilar temperatures.

distances this may be considered as an error of 0.001 cm (for $dC/dx = 10$) in the location of the curve. Taking both welds in consideration this indicates a possible error of ± 0.002 cm or about 5% error in shift.

Errors could also arise due to lack of symmetry in the data (about the $C_0/2$ concentration plane) and due to the variance of the calculated slopes. However, the centroids were usually quite close to the $C_0/2$ concentration and these errors may be considered insignificant compared to errors from other sources.

D. ERRORS IN TIME MEASUREMENT

The duration of experiments was timed to the second. The only significant source of error arose from the occasional changes in specimen current polarity when checking the balance circuit. Specimens were not subjected to reverse polarity for more than a total of 2 minutes, giving a total error of 4 minutes or about -1%.

E. ERRORS IN EFFECTIVE CHARGE

The effective charge is given by the equation:

$$q_{\text{eff}} = \frac{vkT}{DeE} \quad (10)$$

Thus, random errors in effective charge may be calculated approximately from the equation:

$$q_{\text{eff}} = \Delta v + \Delta E + \Delta T + \Delta D \quad (11)$$

where the Δ 's are percentage errors given in Table VII.

A probable random error of 12% is obtained for effective

TABLE VII
Summary of Errors

Source	Probable Random Error %	Limits of Systematic Error %
T	± 0.2	+0.3 -0.6
D	± 2.0	+3.0 -5.0
E	± 2.0	± 3.0
v	± 8.0	+1.0 -0

charge values obtained in the present experiment. This error limit may be assigned to the values in Figure 26. Systematic errors are excluded from this graph since the main aim of the present investigation is to measure the variation of effective charge with temperature and current density. However, it is recognised that the actual charge values could all be as much as 9.3% higher or 6.6% lower than the values calculated.

DISCUSSION

The results of the present investigation show that there is a definite variation of the effective charge with current density during low field electrotransport of carbon in iron, an effect which deviates from the generally accepted electrotransport theories. It would be of great interest to determine whether this variation is peculiar to interstitial iron-carbon alloys, or whether it also occurs in other systems. In most investigations where variations of effective charge with temperature have been reported, different specimen temperatures were attained by the simple expedient of varying the current density. It appears plausible that at least part of the reported charge variation (c.f. Table II) could be due not to the temperature change per se, but rather to the accompanying change in current density. Huntington and Grone¹⁸ have found the effective charge to be independent of current density for self transport in gold. However, the experiments on gold were performed at very high current densities, in the region of 10^4 A cm⁻², which is approximately an order of magnitude higher than the current density levels employed in the present investigation. Figure 26 shows that at current densities of 10^4 and 2×10^4 A cm⁻² the predicted values of carbon effective charge are 1.45 and 1.3 respectively, a variation too small to be detected by the present experimental measurements. Seith and Wever³⁴ have encountered a non linear variation of mobility with applied field in substitutional alloy (Cu-Al) electrotransport at a current density of about 10^4 A cm⁻²

indicating that this phenomenon is not restricted solely to interstitial alloys, and may also occur at high fields.

A. SCATTERING CONSIDERATIONS

The apparent variation of the effective charge with field could be explained fairly simply if it is assumed that the scattering cross section of defects varies with applied field (c.f. Equation 1). This model has some credence for collision processes in plasmas. In ionised gases the scattering cross sections for electron-atom collisions (in inert gases) is small at low fields, increases rapidly to a maximum and then decreases to a low value as the field is increased⁴². This corresponds closely to the variation in effective charge as a function of the applied field observed in this investigation. Such a mechanism would readily permit the evaluation of the true charge from data at different fields, since as the applied field approaches infinity the scattering cross section (and thus the momentum transfer effect) approaches zero, and the effective and true charges become identical. Unfortunately this rather facile explanation is not acceptable. Variations in the scattering cross sections for gases are related to variations in the particle velocities. In a solid metal the electrons are moving with a relatively constant mean velocity of 10^8 cm s⁻¹, and the maximum electron drift velocity due to the applied field is unlikely to have been larger than 10 cm s⁻¹. Thus the applied field makes a negligible contribution to the mean electron velocity, and should not substantially alter the scattering cross section for

electron-ion and hole-ion collisions. For similar reasons the possibility that the effective charge varies as a result of changes in the concentration of electrons or holes, or their effective masses, due to distortion of the Fermi surface by the applied field, is also discounted. The application of the field causes an asymmetry in the electron momentum distribution, which results in the drift velocity, but the corresponding energy change is several orders of magnitude less than the thermal energy contribution, and it is unlikely this would result in a charge carrier concentration change through inter- or intra-band transitions.

B. JUNCTION EFFECTS

A very sensitive dependence of effective charge with applied field could arise from junction effects at the weld interfaces between the alloy and pure iron sections of the wire. This would be in the nature of a p-n effect requiring that a potential barrier be overcome before a current could flow. However, plots of voltage drops within the alloy (ΔV_a) and across the weld (ΔV_w) against current, measured on a typical specimen, were found to be linear, as shown in Figure 28. Thus it is concluded that the electron current was in no way affected by junction effects, though this is no guarantee that the ion current was also unaffected. Moreover, from the slopes in Figure 28, the resistivities of the alloy and weld sections of the wire were calculated and found to agree within 0.6%, which is an indication of the soundness of the weld.

C. DIFFUSIVITY CHANGE CONSIDERATIONS

An alternative approach is to consider the possibility that the diffusivity, through the activation energy or the correlation factor, may depend on the applied field. This does not appear unlikely since the field will have a polarising effect restricting the atom jump directions, and will also induce vacancy motion which can accelerate the ionic diffusion process. Stepper and Wever⁴³ measured extremely high effective charges for several minor components in dilute copper alloys, which they attributed to very small correlation factors and, in one case, short cut diffusion by a dislocation pipe mechanism. For either process acceptable effective charge values could be calculated if it was assumed that in electrotransport the diffusivity was much higher than in normal chemical diffusion. In iron self transport Hering and Wever⁴⁴ found similarly high electrotransport rates and calculated an "effective" electrotransport diffusion activation energy of about $30.5 \text{ kcal mol}^{-1}$, as compared to a value of about 70 kcal mol^{-1} for normal chemical diffusion transport.

In the present investigation it is unlikely that the variation of effective charge is the result of a change of diffusivity with field, for the diffusivities were calculated directly from the penetration curves and the values obtained were found to be in close agreement with published data. Unless it is postulated that the electrotransport and chemical diffusion processes can occur independently at different diffusivities, the apparent variation of the effective charge cannot be attributed to diffusivity changes.

D. PROPOSED TRANSPORT MODEL

The plot of ion velocity against applied field shown in Figure 31 suggests that the electrotransport of carbon may occur by two separate processes; one process causing the initial sharp increase in velocity with applied field saturates at fairly low field strength, while the further subsequent rise in velocity is due to a different electrotransport mechanism. This latter process appears to be the normal interstitial transport mechanism. At fields greater than 0.028 V cm^{-1} the ion velocity is linearly related to the field, and therefore the effective charge for this process is constant, which is in agreement with theoretical predictions.

Although the transport of carbon is considered to occur by purely interstitial motion, and this is undoubtedly the major mechanism in chemical diffusion, some transport will also occur as a result of vacancy diffusion. Carbon atoms may occupy vacant lattice sites, an energetically probable state since lattice strains are thereby reduced, and carbon motion may occur by the interchange of positions of the carbon-vacancy complex with an iron atom. The exact interchange may be a direct interchange affecting only one iron atom, or a rotational mechanism where several iron atoms move. It was noted earlier that iron ions will migrate towards the cathode in self transport of pure iron^{7,32}, and towards the anode in electrotransport of iron-carbon alloys^{35, 36,37}. The mechanism of vacancy migration may be used to explain this change in polarity of the electrotransport direction. Evidently in self transport the ionic charge and hole-ion collision

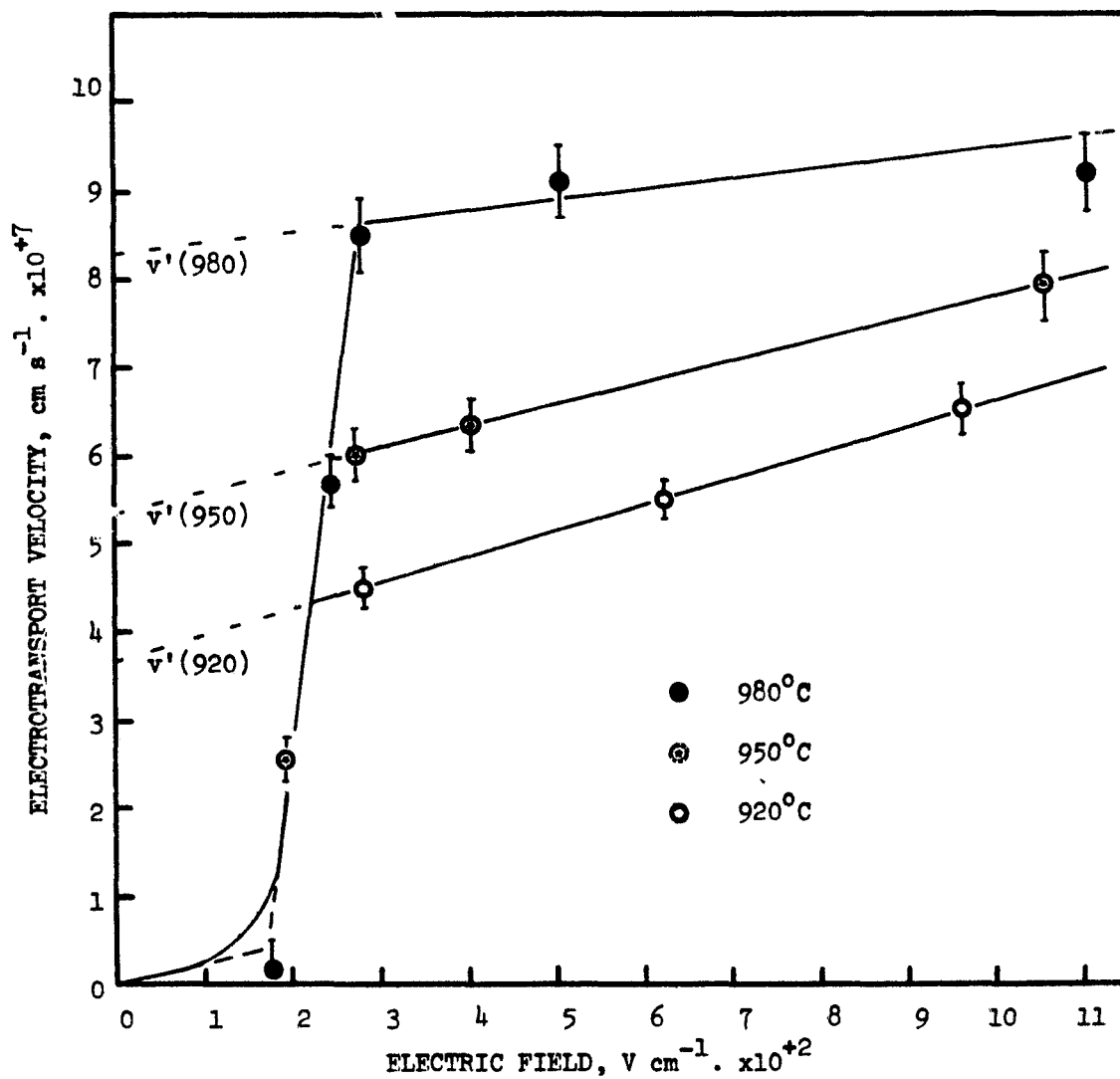


Figure 31. Electrotransport velocity versus applied field at different temperatures.

processes result in a net force on the iron ions in the direction of the applied field. Thus the most probable interchange between an ion and a vacancy is one which results in motion of the ion towards the cathode as shown in Figure 32(a). In an iron-carbon alloy the vacancy may be occupied by a carbon ion. In this case both carbon and iron ions experience cathode directed forces. It appears that the electrotransport force is comparatively higher for the carbon ion than for the iron ion and the most probable interchange is one in which the carbon ion moves in the direction of the cathode, which necessitates iron travelling towards the anode, as shown in Figure 32(b).

The above interchange mechanism for carbon motion could give rise to the initial sudden increase in carbon ion velocity with applied field. Generally most substitutional diffusion processes are considered negligibly slow compared to interstitial transport, but in iron, and particularly in the electrotransport of iron, this does not appear to be the case. Aluminum forms a substitutional alloy with iron, yet its diffusion rate in iron is only one order of magnitude smaller than the interstitial diffusion rates in gamma iron³⁹. Frantsevich et al³⁵ quote electrotransport velocities for iron (in iron-carbon alloys) of $2 \times 10^{-6} \text{ cm s}^{-1}$, which are comparable to interstitial electrotransport velocities for carbon. In iron self transport Hering and Wever⁴⁴ calculated the activation energy for self transport to be less than one half the normal chemical diffusion activation energy; diffusion by a dislocation pipe mechanism was considered to be the cause of the low activation energy. Frantsevich et al³⁶ found that the transport numbers for iron and carbon

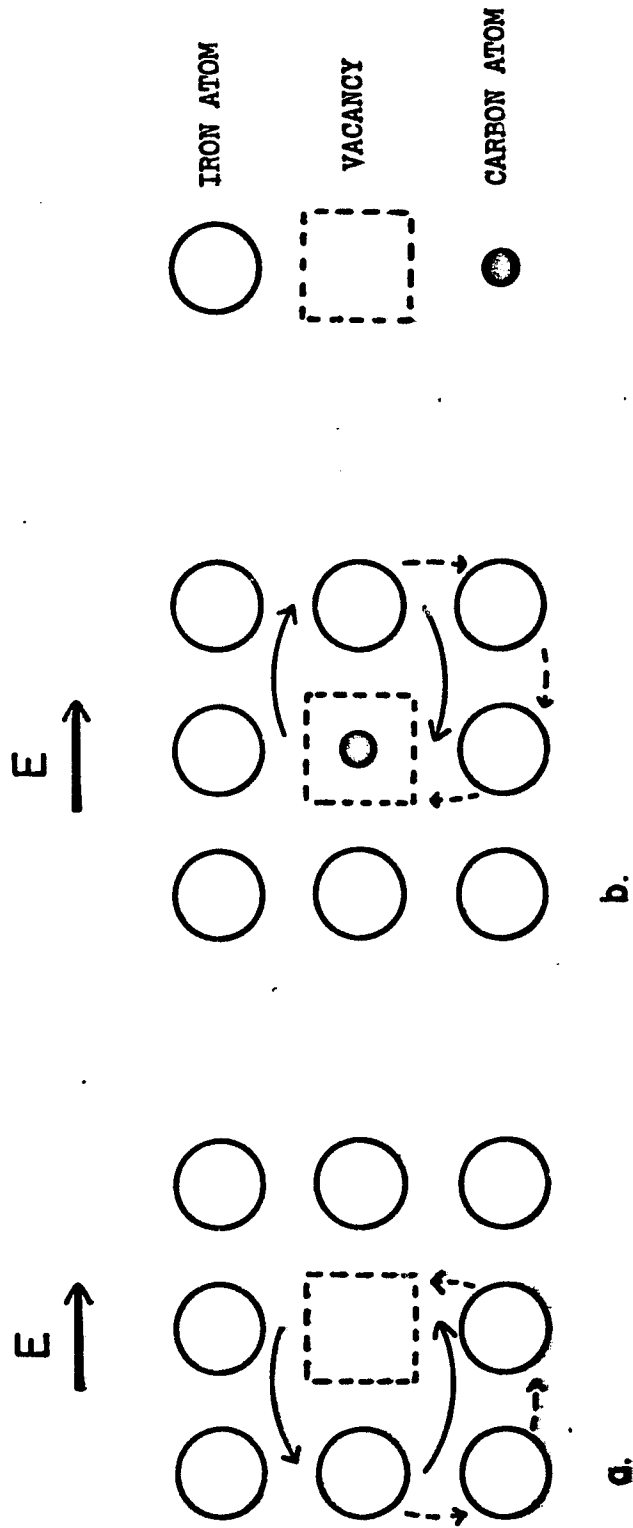


Figure 32. Vacancy interchange mechanism: (a) pure iron
(b) iron-carbon alloy

electrotransport in iron-carbon alloys are of the same order of magnitude. Thus it appears plausible that transport by the interchange mechanism may be comparable in magnitude to the rate of interstitial transport.

Figure 31 suggests that the carbon-vacancy-iron interchange mechanism is activated by a small field, but that once fully activated it is no longer responsive to further increase in applied field. Normally the probability of a diffusion jump occurring in a given direction is an exponential function of the force on the ion in that direction. It is proposed that the interchange mechanism is extremely sensitive to the applied field; at fields as low as 0.028 V cm^{-1} the probability of a carbon jump toward the cathode is almost one hundred per cent. Applied fields greater than 0.028 V cm^{-1} do not substantially increase this probability, and the total contribution to the electrotransport velocity due to the quasi-substitutional interchange process is determined by its activation energy and the specimen temperature. In Figure 31 the intercepts $v'(T)$ represent the contribution of this mechanism to electrotransport. A plot of $\log v'(T)$ versus T^{-1} , shown in Figure 33, is reasonably linear. Assuming that $v'(T) = A \cdot \exp(-Q_v/RT)$, the activation energy for this process, Q_v , was calculated to be 42 kcal mol^{-1} . This value is about the correct magnitude for vacancy diffusion in metals (Honeycombe⁴⁵) and supports the hypothesis that a vacancy interchange mechanism contributes to electrotransport. Presumably Q_v comprises the activation energies for both vacancy formation and vacancy motion.

Several of the assumptions made in proposing a relatively fast vacancy transport mechanism may be subject to criticism.

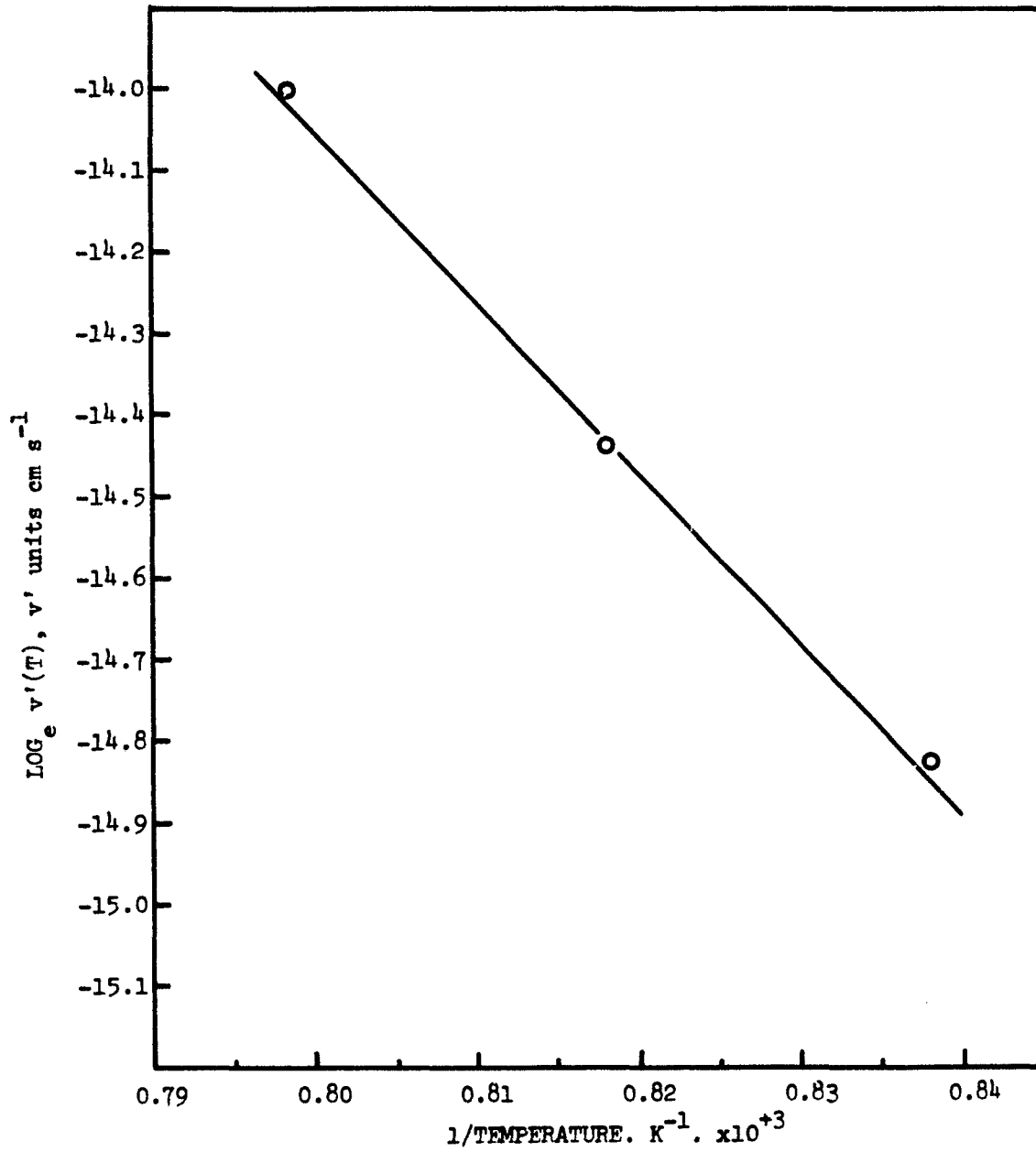


Figure 33. The non interstitial contribution to the electrotransport velocity as a function of temperature.

In particular the proposed very sensitive dependence of such a mechanism on the applied field is difficult to explain satisfactorily. It is possible that the field might distort the spatial distribution of shielding electrons in the neighbourhood of ions or vacancies, making the direction of the applied field a highly preferred direction for diffusion jumps. This would result in very small jump correlation factors, as postulated by Stepper and Wever⁴³ in explaining the very rapid transport they encountered in copper alloys.

The fraction of vacancies in metals at 1000°C is in the order of 10^{-5} (or 0.001% of the lattice sites)⁴⁶ which is considerably less than the concentration of carbon in the alloys used in the present experiments. Moreover, not all vacancies will be occupied by carbon atoms. Thus it could be argued that only a minute fraction of carbon atoms could move by the vacancy mechanism. This is a valid argument, and not one to be easily confuted. However, it might be suggested that the strain energy contributed to the lattice by interstitials may be reduced by the introduction of a vacancy in the vicinity of an interstitial atom, so that in order to lower the lattice strain energy an iron-carbon alloy may contain a larger equilibrium total number of vacancies than the pure metal. Unfortunately, exact data of this nature is not readily available and an accurate estimate of the vacancy concentration cannot be presented.

There exists the possibility that the relatively fast electrotransport at low fields is not attributable to a vacancy interchange, but rather to a completely different mechanism such as dislocation pipe diffusion (c.f. Hering and Wever⁴⁴) or grain

boundary diffusion. It is interesting to note that for grain boundary diffusion of iron the activation energy is 40 kcal mol^{-1} (Shewmon⁴⁷) which agrees closely with the activation energy of 42 kcal mol^{-1} obtained from Figure 33. In the present investigation the grain size of the alloys was about 80 microns and at the high temperatures of the experiments it is unlikely that grain boundary diffusion would have contributed substantially to the total diffusion transport. Moreover, it may logically be expected that carbon grain boundary diffusion would have an activation energy smaller or at least comparable to the interstitial activation energy of 29 kcal mol^{-1} . It may, however, be postulated that the fast low field electrotransport could be related to grain boundary diffusion if carbon and iron atoms move in synchronism (with an activation energy of 40 kcal mol^{-1}) by some field dependent interchange mechanism. Since grain boundaries may be viewed as an agglomeration of vacancies, grain boundary electrotransport would thus be only a more general case of the vacancy interchange mechanism discussed previously. The difficulties already encountered in attempting to explain the field effects in vacancy interchange electrotransport would be just as severe in the case of grain boundary transport.

E. EFFECTIVE CHARGE FOR INTERSTITIAL TRANSPORT

The model of carbon-vacancy-iron interchange seems the most plausible explanation for the relatively large electrotransport velocities occurring at very low applied fields. However, it is possible that some other short circuit diffusion process,

possessing the properties of easy activation and saturation by the field and having an activation energy of approximately 42 kcal mol^{-1} , could operate and contribute to electrotransport. In any case there is little doubt that the variation of velocity with applied field beyond 0.028 V cm^{-1} may be attributed primarily to normal interstitial transport. For this region the ion velocity may be expressed as follows:

$$v = \frac{eED}{kT} \cdot q_{\text{eff}(i)} + v'(T), \quad \text{for } E = 0.028 \text{ V cm}^{-1} \quad (12)$$

where $q_{\text{eff}(i)}$ is the effective charge for purely interstitial electrotransport and $v'(T)$ is the intercept on the v -axis at $E = 0$ as shown in Figure 31 and represents the contribution of a vacancy mechanism to the ion velocity. The charge may be calculated from either of the following equations:

$$q_{\text{eff}(i)} = \frac{kT}{eD} \cdot \frac{(v - v'(T))}{E}, \quad \text{for } E = 0.028 \text{ V cm}^{-1} \quad (13)$$

or

$$q_{\text{eff}(i)} = \frac{\partial v}{\partial E} \cdot \frac{kT}{eD} \quad (14)$$

Using Equation (14) the effective charges for interstitial transport were calculated and are given in Table VIII; the errors shown in Table VIII were estimated from individual evaluations of $q_{\text{eff}(i)}$ using Equation (13).

These results are in fair agreement with those quoted by Darken et al.¹⁰ and Frantsevich et al.³⁶ (see Table II). Moreover, whereas the overall effective charge values showed little variation with temperature (except, perhaps, for the values at highest current densities), the calculated effective charge values for

TABLE VIII

Effective Charge Values for Purely
Interstitial Electrotransport

Temperature $T^{\circ}\text{C}$	Effective Charge $q_{\text{eff}(i)}$	Probable Error
920	2.45	± 0.05
950	1.51	± 0.02
980	0.57	± 0.10

interstitial transport show a pronounced temperature dependence. Frantsevich and Kovenskii³⁸ have found the effective charge of carbon in iron to be a hyperbolic function of the factor $(T + \rho_0 / \alpha)^{-1}$, and calculated a true charge value for carbon in gamma iron. A similar analysis is not feasible with the present results; more data than that available would be required to establish the exact relation between the interstitial effective charge and temperature. However, the calculated interstitial effective charges appear to be extremely sensitive to temperature, perhaps more sensitive than a hyperbolic dependence would warrant. Bibby et al⁹ found the change in charge from 842°C to 902°C to be much more pronounced than the change from 902°C to 950°C, as shown in Table II. Kalinivich¹² and Frantsevich et al³⁶ encountered discordantly low values of charge at 1050°C, and Darken et al¹⁰ were unable to establish a consistent temperature dependence at all. Thus it appears plausible that though the effective charge may be hyperbolically related to temperature over a relatively small temperature range, over a wide range the relation may not be a simple monotonic one. It is difficult to analyze and compare results in the literature with confidence since it is seldom known whether the effective charges reported were affected by the field dependence observed in the present investigation.

The pronounced variation of effective charge with temperature (for interstitial transport) may result from changes in the electron/hole concentration ratio and the effective masses of electrons and holes. Such an effect was suggested earlier as a possible explanation for the negative effective charges found in

p-conducting alloys (c.f. Kuz'menko et al^{29,30}) and the opposite polarities of the effective charge of copper at temperatures below and above 1000°C (c.f. Wever³¹ and Grone³³).

The low effective charges obtained for carbon interstitial transport (i.e. $q_{eff(i)} \approx +4$) indicates that the hole-ion momentum transfer is probably smaller than the electron-ion momentum transfer. Bibby et al⁹ arrived at the opposite conclusion; the large positive effective charge ($q_{eff} \approx +4$) they obtained for carbon transport in gamma iron seemed to indicate that holes were the predominant charge carriers in the collision process. Presumably, where hole and electron momentum transfer contributions are identical a true charge of about +4 would be measured (c.f. Equation 1).

It is to be expected that at very high fields the overall effective charge should approach the interstitial effective charge, since at high fields $v \gg v'(T)$ and $\partial v / \partial E \approx v/E$. It is interesting to note that in Figure 26 the best fit lines to the high field points ($E > 0.028 \text{ V cm}^{-1}$) at 920, 950 and 980°C intersect the q_{eff} -axis at about 2.5, 1.2 and 0.5 respectively. These values are comparable to the interstitial effective charges shown in Table VIII. Thus for fields of the order of 10^4 A cm^{-2} the interchange contribution is relatively small and little error is incurred in neglecting it in the calculation of charge. However, this will not always be the case, and it is quite possible that in some alloys short cut diffusion may occur causing a variation of effective charge with applied field even at high field strengths. Where accurate measurements of effective charge are required the possibility of a field dependence should be carefully investigated.

CONCLUSIONS

1. The effective charge of carbon in gamma iron is a function of the applied electric field, but this field dependence is only appreciable at low fields.
2. Electrotransport of carbon appears to occur by two independent processes: the normal interstitial transport and a postulated vacancy interchange mechanism.
3. The interstitial transport velocity is proportional to the applied field in accordance with accepted theories. An interstitial transport effective charge may be calculated.
4. Vacancy transport is activated by a field of 0.028 V cm^{-1} , but is field independent at higher fields. The maximum contribution of this process to the total velocity varies with temperature, and its rate appears to be exponentially related to an activation energy of 42 kcal mol^{-1} .
5. At fields of about 0.028 cm^{-1} the carbon electrotransport is almost entirely determined by vacancy transport. As the applied field is increased the interstitial transport becomes significant and may become dominant at fields larger than 1.0 V cm^{-1} .
6. The interstitial effective charge is strongly temperature dependent, increasing as the temperature is decreased.
7. The low effective charge values for carbon interstitial electrotransport suggest that the electron-ion momentum transfer exceeds the hole-ion momentum transfer.

8. Diffusion coefficients calculated from carbon penetration curves are in fair agreement with published data and indicate that in chemical diffusion the only significant process was interstitial migration.

BIBLIOGRAPHY

1. Bibby, M.J., and Youdelis, W.V., Can. J. Phys., 1966, 44, 2363.
2. Smolin, M.D., and Frantsevich, I.N., Soviet Physics - Solid State, 1962, 3, 1536.
3. Smolin, M.D., *ibid.*, 1963, 5, 1151.
4. Smolin, M.D., *ibid.*, 1966, 7, 1758.
5. Smolin, M.D., *ibid.*, 1967, 9, 1415.
6. Kalinovich, D.F., Kovenskii, I.I., and Smolin, M.D., *ibid.*, 1968, 10, 447.
7. Kalinovich, D.F., Kovenskii, I.I., and Smolin, M.D., *ibid.*, 1969, 10, 1589.
8. Kalinovich, D.F., Kovenskii, I.I., and Smolin, M.D., *ibid.*, 1969, 10, 1946.
9. Bibby, M.J., Hutchison, L.C., and Youdelis, W.V., Can. J. Phys., 1966, 44, 2375.
10. Dayal, P. and Darken, L.S., J. of Metals, Trans. AIME, 1950, 188, 1156.
11. Frantsevich, I.N., Kalinovich, D.F., and Kovenskii, I.I., Fiz. Metal Metalloved., 1959, 4 574.
12. Kalinovich, D.F., Soviet Physics - Solid State, 1961, 3, 812.
13. Ficks, W.B., Soviet Physics - Solid State, 1959, 1, 14.
14. Glinchuck, M.D., Ukrain. Fiz. Zhur., 1959 4 684.
15. Verhoeven, J., Metallurgical Reviews, 1963, 8, #31, 311.
16. Klemm, A., Z. Naturforsch., 1953 (a) 8, 393.
17. Mangelsdorf, P.C., "Electrolysis and Dissusion in Liquid Alloys", (Met. Soc. AIME Conference 7), 1961, p.429.
18. Huntington, H.B., and Grone, A.R., J. Phys. Chem. Solids, 1961, 20, 76.
19. Huntington, H.G., and Ho, S-C., J. Phys. Soc. Japan, 1963, 18, Sup.II, 202.

Bibliography (cont'd)

- 20 Bosvieux, C. and Friedel, J., Phys. Chem. Solids, 1962, 23, 123.
- 21 Boltaks, B.I., "Diffusion in Semiconductors", Academic Press, New York, 1963.
- 22 Metals Handbook, ASM, 1964.
- 23 Gerardin, M., Compt. Rend., 1861, 53, 727.
- 24 Seith, W. and Kubaschewski, O., Z. Electrochem., 1934, 40, 829.
- 25 Seith, W. and Daur, Th., Z. Electrochem., 1938, 44, 256.
- 24 Johnson, R.P., Phys. Rev., 1938, 53, 766.
- 27 Johnson, R.P., ibid., 1938, 54, 459.
- 28 Kuz'menko, P.P., and Khar'kov, E.I., Ukrain. Fiz. Zhur., 1958, 3, 528.
- 29 Kuz'menko, P.P., and Khar'kov, E.I., ibid, 1959, 4, 537.
- 30 Kuz'menko, P.P., and Khar'kov, E.I., ibid, 1960, 5, 428.
- 31 Wever, H., Z. Electrochem., 1956, 60, 1170.
- 32 Wever, H., "The Physical Chemistry of Metallic Solutions and Intermetallic Compounds", (London, H.M. Stat. Office), Vol.1, Paper 2L. 1959.
- 33 Grone, A.R., J. Phys. Chem. Solids, 1961, 20, 88.
- 34 Seith, W. and Wever, H., Z. Electrochem., 1953, 57, 891.
- 35 Frantsevich, I.N., Kalinovich, D.F., Kovenskii, I.I. and Pen'kovsky, V.V., Soviet Physics - Doklady, 1958, 3, 842.
- 36 Frantsevich, I.N., Kalinovich, D.F., Kovenskii, I.I. and Smolin, M.D., Soviet Physics - Solid State, 1959, 1, 58.
- 37 Gertstriken, S.D., Dakhtyar, I.Y., Mikhalenkov, V.S. and Fal'chenko, V.M., Ukrain. Fiz. Zhur., 1961, 6, 129.
- 38 Frantsevich, I.N. and Kovenskii, I.I., Dopovidi Akad., Nauk. Ukr. RSR, 1961, 9, 1169.
- 39 Smithells, C.J., "Metals Reference Book", 1962.
- 40 Wells, C., Batz, W., and Mehl, F., Trans. AIME, 1952, 188, 553.

Bibliography (cont'd)

- 41 Hutchinson, L.C., Masters Thesis, University of Alberta, 1965.
- 42 Delcroix, J.L., "Introduction to the Theory of Ionized Gases", Interscience, New York, 1960.
- 43 Stepper, H.J. and Wever, H., J. Phys. Chem. Solids, 1967, 28, 1103.
- 44 Hering, H. and Wever, H., Acta Met., 1967, 15, 377.
- 45 Honeycombe, R.W.K., "The Plastic Deformation of Metals", Arnold Ltd., London, 1968.
- 46 Kittel, C., "Introduction to Solid State Physics", J.Wiley & Son, Inc., London, 1961.
- 47 Shewmon, P.G., "Diffusion in Solids", McGraw-Hill, New York, 1963.
- 48 Neville, A.M. and Kennedy, J.G., "Basic Statistical Methods", International Textbook, 1964.
- 49 Darken, L.S. and Gurry, R.W., "Physical Chemistry of Metals", McGraw-Hill, New York, 1953.

APPENDIX I

Analysis of Armco Iron

Impurity Element	Concentration wt %
C	0.012
Mn	0.06
P	0.012
S	0.013
Ni	0.04
Cr	0.03
Cu	0.08
Si	0.020
Al	0.010
N	0.007
O	0.053

The above analysis was obtained from Chicago Spectro
Analysis Incorporated.

APPENDIX II

Concentration Calculation

The relationship between the hardness of iron-carbon martensite and the carbon concentration shown in Figure 11 can be approximated by a straight line with the following equation:

$$\text{CONC} = 1.041 \times 10^{-3} \times \text{VPH} - 0.2977.$$

where CONC is the concentration of carbon in weight per cent, and VPH is the Vickers Pyramid Hardness number.

A simple computer program incorporating this equation was used to convert indentation diagonals to concentration values. The concentrations were expressed as atomic per cent values, these units being more suitable to the plotting of diffusion penetration curves. The positions of the indentations were given with reference to the welds and expressed in centimeters.

```

*      JOB      E A FALGUERO  LNG MAT  ELECTROTRANSPORT ANALYSIS
      PUNCH,12H SERIES C
      3 READ,AO,CO,RN
        IF(RN)5,4,5
      4 STOP
      5 PUNCH 6,RN
      6 FORMAT(11HRUN NUMBER ,F5.2)
      PUNCH,5UH  X ANODE  X CATHODE  C CONCENTRATION
      10 READ,X,DIA
        IF(X)20,3,20
      20 VPH = 927200./DIA**2
        CONC = .001041 * VPH - .2977
        APC = 100.*CONC/(CONC + .21504 * (100. - CONC))
        CENT = (AO + CO) / 2.
        IF(X-CENT)25,25,30
      25 X = (X-AO) * 2.54
        PUNCH 27,X,APC
      27 FORMAT(F15.8,15H
                ,F15.8)
        GO TO 10
      30 X = (CO - X) * 2.54
        PUNCH 32,X,APC
      32 FORMAT(15H
                ,F15.8,F15.8)
        GO TO 10
      END

```

APPENDIX III

Conversion Table

A conversion table relating indentation diagonals, hardnesses, and compositions was calculated. The following equations were used:

$$VPH = \frac{9.272 \cdot 10^5}{(DIA)^2}$$

$$WPC = 1.041 \cdot 10^{-3} \times VPH - 0.2977$$

$$APC = \frac{100 \cdot WPC}{(WPC + 0.21504 \cdot (100 - WPC))}$$

where
DIA = Mean indentation diagonal at 500 gm load
VPH = Vickers Pyramid Hardness number
WPC = Carbon concentration in weight per cent
APC = Carbon concentration in atomic per cent

DIA	VPH	WPC	APC
32.00	908.5	.6449	2.9300
32.30	886.7	.6275	2.8826
32.70	867.1	.6050	2.7525
33.00	851.4	.5886	2.6797
33.30	836.2	.5727	2.6086
33.70	816.4	.5522	2.5171
34.00	802.1	.5375	2.4504
34.30	788.1	.5227	2.3883
34.70	770.0	.5089	2.3010
35.00	756.9	.4902	2.2396
35.30	744.1	.4769	2.1796
35.70	727.5	.4596	2.1022
36.00	715.4	.4471	2.0456
36.30	703.7	.4348	1.9904
36.70	688.4	.4189	1.9186
37.00	677.3	.4074	1.8665
37.30	666.4	.3961	1.8155
37.70	652.4	.3814	1.7495
38.00	642.1	.3707	1.7010
38.30	629.5	.3555	1.6229
39.00	609.6	.3369	1.5476
39.50	594.3	.3209	1.4751
40.00	579.5	.3056	1.4053
40.50	565.3	.2908	1.3379
41.00	551.6	.2765	1.2720
41.50	538.4	.2627	1.2102
42.00	525.6	.2495	1.1497
42.50	513.3	.2367	1.0912
43.00	501.5	.2243	1.0347
44.00	478.9	.2009	.9273
45.00	457.9	.1789	.8268
46.00	438.2	.1585	.7326
47.00	419.7	.1392	.6443
48.00	402.4	.1212	.5613
49.00	386.2	.1043	.4832
50.00	370.9	.0884	.4097
51.00	356.5	.0734	.3404
52.00	342.9	.0593	.2750
53.00	330.1	.0459	.2132

APPENDIX IV

Evaluation of Centroids and Slopes

One of the best methods of fitting a line to a set of experimental points is a regression analysis. In the present analysis only the hardness points falling within the concentration limits $\frac{1}{2}C_0$ and $\frac{3}{4}C_0$ were weighted since this is the most sensitive region of the penetration curve and the shift between anode and cathode curves would be most accurately measured in the vicinity of the $C_0/2$ concentration. Moreover at very high and very low concentrations the hardness measurements become less accurate than in the medium concentration regions due to the increased reading error (smaller diagonals) and distortion of the indentations respectively.

Advantage was taken of the fact that over the region stipulated the diffusion penetration curve could be approximated by a straight line without incurring large errors (see Figure 34). Neville and Kennedy⁴⁸ show that the straight line approximation to a set of experimental points is given by an equation of the type:

$$y = \frac{\sum XY}{\sum X^2} \cdot x$$

where (Y,X) are the co-ordinates of the points relative to the centroid (\bar{Y}, \bar{X}) used as origin. The co-ordinates of the centroids are the mean y and x values for all the points.

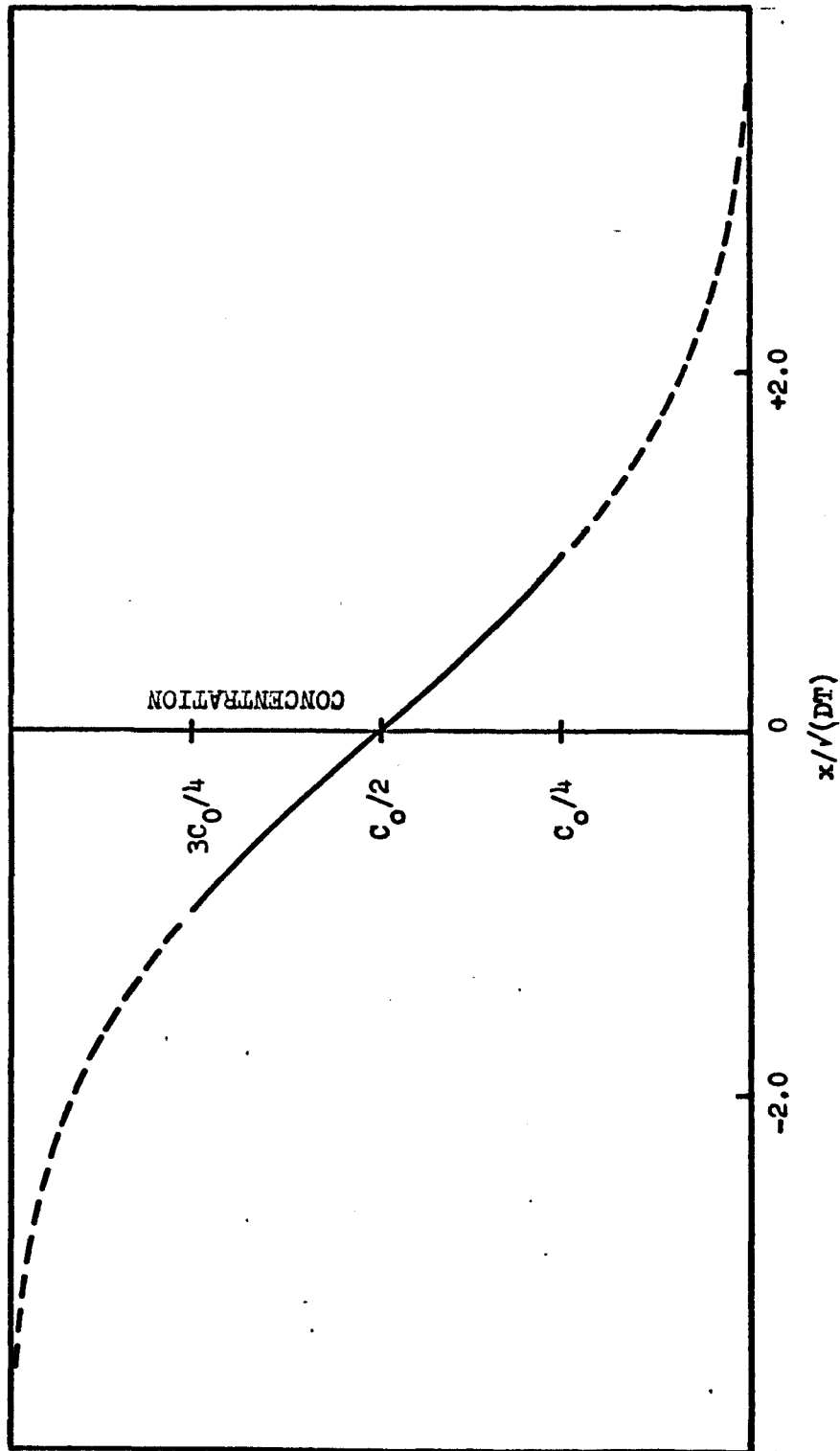


Figure 34. Theoretical diffusion penetration curve (Darken and Gurry⁴⁹).

$$\bar{y} = \sum_{i=1}^n y_i/n, \quad \bar{x} = \sum_{i=1}^n x_i/n,$$

for a sample of n points.

For each set of data the centroids and the slopes of the penetration curves were calculated. A trial run on standard diffusion data taken from Darken and Gurry⁴⁹ indicated that the slope given by the straight line approximation differed from the maximum theoretical slope (at $C_0/2$) by a factor of 1.05. This factor was introduced as a correction in the evaluation of the slope. Computer programs were used in these calculations.

It must be emphasized that this technique is not considered to be a strict statistical analysis, but rather a simple approximation. The centroids provided anchor points and the slopes were used as guidelines in the region of concentration near $C_0/2$. The rest of the penetration curve was drawn freehand as the best fit line to the data.

```

*          JO3          FALQUERO.  CENTROIDS
PUNCH,40H POLARITY  RUN  X-CENT  Y-CENT
2 READ,PN,RN,POL
  IF(PN)4,4,5
4 STOP
5 SMX = 0.0
  SMY = 0.0
7 READ,X,Y
  SMX = SMX + X
  SMY = SMY + Y
  IF(X)7,B,7
8 XC = SMX / PN
  YC = SMY / PN
  IF(POL)10,10,20
10 PUNCH 15,RN,XC,YC
15 FORMAT(10H CATHODE ,F7.2,F10.5,F10.5)
  GO TO 2
20 PUNCH 25,RN,XC,YC
25 FORMAT(10H ANODE ,F7.2,F10.5,F10.5)
  GO TO 2
  END

```

```
*      JOB      FALQUERO.  SLOPES  RUN      X-CENT      Y-CENT      SLOPE      COR.SL.
PUNCH,56H POLARITY
2 READ,PN,RN,POL
  IF(PN)4,4,5
4 STOP
5 READ,XC,YC
  SPR = 0.0
  SXQ = 0.0
7 REAL,X,Y
  IF(X)11,8,11
11 XN = X - XC
  YN = Y - YC
  PR = XN*YN
  XQ = XN*XN
  SPR = SPR + PR
  SXQ = SXQ + XQ
  GO TO 7
8 B = SPR / SXQ
  TB = 3*1.05
  IF(POL)10,10,20
10 PUNCH15,RN,XC,YC,B,TB
15 FORMAT(10H CATHODE ,F7.2,F10.4,F10.4,F10.4,F10.4)
  GO TO 2
20 PUNCH25,RN,XC,YC,B,TB
25 FORMAT(10H ANODE ,F7.2,F10.4,F10.4,F10.4,F10.4)
  GO TO 2
  END
```

APPENDIX V

Sample Calculation

Specimen #10

Temperature (T) = $950^{\circ}\text{C} = 1223\text{ K}$

Time (t) = $2.34 \times 10^4\text{ s}$

Field (E) = 10.58 V m^{-1}

Current (I) = 9.97 A

Diffusivity, mean (D) = $1.70 \times 10^{-11}\text{ m}^2\text{ s}^{-1}$

Electronic charge (e) = $1.592 \times 10^{-19}\text{ coulomb}$

Boltzman constant (k) = $1.38 \times 10^{-23}\text{ joules K}^{-1}$

Shift = $0.037\text{ cm} = 3.7 \times 10^{-4}\text{ m}$

Ion velocity (v) = $\frac{3.7 \times 10^{-4}}{2 \times 2.34 \times 10^4}$

= $7.9 \times 10^{-9}\text{ m s}^{-1}$

Effective charge (q_{eff}) = $\frac{vkT}{DeE} = \frac{7.9 \times 10^{-9} \times 1.38 \times 10^{-23} \times 1223}{1.7 \times 10^{-11} \times 1.592 \times 10^{-19} \times 10.58}$

= 4.46

Current density (J) = $\frac{9.97}{(2.54 \times 0.045)^2} \cdot \frac{4}{\pi}$

= $971\text{ A cm}^{-2} = 9.71 \times 10^6\text{ A m}^{-2}$

$1/J = 1.03 \times 10^{-3}\text{ cm}^2\text{ A}^{-1} = 1.03 \times 10^{-7}\text{ m}^2\text{ A}^{-1}$

$$\begin{aligned}
 \text{Resistivity } (\rho) &= \frac{E}{J} = 10.58 \times 10^{-2} \times 1.03 \times 10^{-3} \\
 &= 108.97 \text{ micro-ohm cm} \\
 &= 1.0897 \times 10^{-6} \text{ ohm m}
 \end{aligned}$$

Diffusivity, calculated.

$$DT = \frac{0.564 \cdot C_o}{\text{Slope} \cdot 2} = \frac{0.282 \times 2.0}{8.71} = 0.0647$$

$$Dt = 41.9 \times 10^{-4}$$

$$D = \frac{41.9 \times 10^{-4}}{2.34 \times 10^4} = 1.79 \times 10^{-7} \text{ cm}^2 \text{ s}^{-1}$$

$$= 1.79 \times 10^{-11} \text{ m}^2 \text{ s}^{-1}$$

VITA AUCTORIS

Birth: Funchal, Madeira, January 1, 1941.

High School: Gibraltar Grammar School, Gibraltar.
1951 to 1959

Universities: University of Liverpool, Liverpool, England
September 1960-July 1963, B.Sc. Ord. Physics.
September 1963-July 1964, B.Sc. Hons. Metallurgy.

University of Alberta, Edmonton, Alberta, Canada.
September 1964-December 1965, M.Sc. Metallurgy.